

## RESEARCH ARTICLE

10.1002/2015JG002915

## Key Points:

- CH<sub>4</sub> and N<sub>2</sub>O emissions in direct-seeded rice fields were estimated by simulation modeling
- Simulated growing season CH<sub>4</sub>, but not fallow CH<sub>4</sub> and annual N<sub>2</sub>O fluxes, matched observed fluxes
- Some specific management effects on fluxes were not well represented in the model

## Correspondence to:

M. B. Simmonds,  
mbsimmonds@ucdavis.edu

## Citation:

Simmonds, M. B., C. Li, J. Lee, J. Six, C. van Kessel, and B. A. Linquist (2015), Modeling methane and nitrous oxide emissions from direct-seeded rice systems, *J. Geophys. Res. Biogeosci.*, 120, 2011–2035, doi:10.1002/2015JG002915.

Received 12 JAN 2015

Accepted 10 SEP 2015

Accepted article online 19 SEP 2015

Published online 21 OCT 2015

## Modeling methane and nitrous oxide emissions from direct-seeded rice systems

Maegen B. Simmonds<sup>1</sup>, Changsheng Li<sup>2</sup>, Juhwan Lee<sup>3</sup>, Johan Six<sup>3</sup>, Chris van Kessel<sup>1</sup>, and Bruce A. Linquist<sup>1</sup>

<sup>1</sup>Department of Plant Sciences, University of California, Davis, California, USA, <sup>2</sup>Institute for the Study of Earth, Oceans, and Space, University of New Hampshire, Durham, New Hampshire, USA, <sup>3</sup>Department of Environmental Systems Science, Swiss Federal Institute of Technology, ETH Zurich, Zurich, Switzerland

**Abstract** Process-based modeling of CH<sub>4</sub> and N<sub>2</sub>O emissions from rice fields is a practical tool for conducting greenhouse gas inventories and estimating mitigation potentials of alternative practices at the scale of management and policy making. However, the accuracy of these models in simulating CH<sub>4</sub> and N<sub>2</sub>O emissions in direct-seeded rice systems under various management practices remains a question. We empirically evaluated the denitrification-decomposition model for estimating CH<sub>4</sub> and N<sub>2</sub>O fluxes in California rice systems. Five and nine site-year combinations were used for calibration and validation, respectively. The model was parameterized for two cultivars, M206 and Koshihikari, and able to simulate 30% and 78% of the variation in measured yields, respectively. Overall, modeled and observed seasonal CH<sub>4</sub> emissions were similar ( $R^2 = 0.85$ ), but there was poor correspondence in fallow period CH<sub>4</sub> emissions and in seasonal and fallow period N<sub>2</sub>O emissions. Furthermore, management effects on seasonal CH<sub>4</sub> emissions were highly variable and not well represented by the model (0.2–465% absolute relative deviation). Specifically, simulated CH<sub>4</sub> emissions were oversensitive to fertilizer N rate but lacked sensitivity to the type of seeding system (dry seeding versus water seeding) and prior fallow period straw management. Additionally, N<sub>2</sub>O emissions were oversensitive to fertilizer N rate and field drainage. Sensitivity analysis showed that CH<sub>4</sub> emissions were highly sensitive to changes in the root to total plant biomass ratio, suggesting that it is a significant source of model uncertainty. These findings have implications for model-directed field research that could improve model representation of paddy soils for application at larger spatial scales.

### 1. Introduction

Conventional agriculture is now the largest anthropogenic source of methane (CH<sub>4</sub>) and nitrous oxide (N<sub>2</sub>O) emissions [Ciais *et al.*, 2013]. Emissions of CH<sub>4</sub> are mainly due to livestock rearing and rice (*Oryza sativa* L.) cultivation, whereas N<sub>2</sub>O emissions are mainly due to extensive use of chemical fertilizer inputs. Greenhouse gas (GHG) emissions from the agricultural sector account for only 10–12% of total anthropogenic GHG emissions (CH<sub>4</sub>, N<sub>2</sub>O, and CO<sub>2</sub>) [Smith *et al.*, 2007] but are responsible for 38% and 59% of global anthropogenic CH<sub>4</sub> and N<sub>2</sub>O emissions, respectively [Ciais *et al.*, 2013]. Therefore, CH<sub>4</sub> and N<sub>2</sub>O are the most prominent GHGs in agriculture, with radiative forcing potentials of 34 and 298 times greater than CO<sub>2</sub> on a 100 year timescale [Myhre *et al.*, 2013], respectively. Also, agricultural soils have high potential for GHG mitigation as agriculture accounts for 40–50% of global land surface area [Smith *et al.*, 2007]. Clearly, a major challenge for agriculture is to decrease the emission of non-CO<sub>2</sub> GHG while sequestering C in the soil to mitigate climate change.

It is important to consider both CH<sub>4</sub> and N<sub>2</sub>O in evaluating GHG mitigation potentials of management strategies for rice cultivation. In general, the contribution of CH<sub>4</sub> emissions to the net global warming potential of rice systems outweighs N<sub>2</sub>O due to the favorably low redox conditions for CH<sub>4</sub> production in continuously flooded rice paddies [Linquist *et al.*, 2012b; Hou *et al.*, 2000]. In O<sub>2</sub>-depleted soil conditions, methanogenic bacteria decompose organic matter, with the symbiotic cooperation of other bacteria types (i.e., hydrolytic and fermenting bacteria), producing CH<sub>4</sub> [Conrad, 2005]. The fate of CH<sub>4</sub> is either oxidation to CO<sub>2</sub> by methanotrophic bacteria depending on the presence of O<sub>2</sub> [Eller and Frenzel, 2001] or release to the atmosphere via diffusion, ebullition, or transport through the aerenchyma system of the rice plants [Holzapfel-Pschorn *et al.*, 1986; Tyler *et al.*, 1997; Yu *et al.*, 1997]. Emissions of N<sub>2</sub>O generally occur under moderate soil moisture conditions when redox levels are not sufficiently low for complete denitrification to occur [Ciarlo *et al.*, 2007].

Thus, in rice systems  $\text{N}_2\text{O}$  emissions tend to occur in discrete peaks during field drainage cycles or precipitation events when fields are already drained [Adviento-borbe *et al.*, 2013; Pittelkow *et al.*, 2013]. As a result,  $\text{CH}_4$  and  $\text{N}_2\text{O}$  emissions generally have an inverse relationship [Hou *et al.*, 2000]. Thus, mitigation practices that target  $\text{CH}_4$  emissions alone (e.g., dry seeding, midseason drainage, alternate wet drying) may have potential to increase  $\text{N}_2\text{O}$  emissions substantially.

The Intergovernmental Panel on Climate Change (IPCC) has established methodologies for calculating GHG emissions with various levels of complexity [Lasco *et al.*, 2006], ranging from Tier 1, default emission factors for specific management practices, to Tier 3 approaches that utilize process-based models that attempt to account for the interrelationships and interactions between management practices, site-specific properties, and the biogeochemical processes involved. The effects of management practices on  $\text{CH}_4$  and  $\text{N}_2\text{O}$  emissions are strongly affected by the soil environment and climate in which they are tested. Various process-based models, including “denitrification-decomposition” (DNDC) [Li, 2000], have been developed and tested to predict trace gas emissions from individual agricultural fields with the capacity to scale up to regional and national levels.

In the U.S., California is the first state to pass legislation (Global Warming Solutions Act of 2006, Assembly Bill 32) setting an enforceable cap on statewide GHG emissions from major industries, with penalties for noncompliance, which has produced a C market for offset projects in industry. A GHG emissions accounting protocol for rice cultivation (i.e., Rice Cultivation Project Protocol, version 1.1, 2013), available from the Climate Action Reserve (<http://www.climateactionreserve.org/>), is one of the offset projects under development. In the U.S., rice cultivation is specifically responsible for 3.7% of agricultural  $\text{CH}_4$  emissions with a current estimate of  $0.3 \text{ Tg CH}_4 \text{ yr}^{-1}$  [United States Environmental Protection Agency, 2014]. The process-based DNDC model is proposed for use to estimate GHG mitigation potentials of C offset projects. The ultimate application of DNDC is scaling up from site mode to simulate trace gas emissions at regional levels. However, an evaluation of its strengths and limitations at the field scale using independent validation data is needed before predictions of C offsets at the field scale or GHG inventories at the national level can be made with confidence. The environmental success of the C trading market and its protocols for quantifying C offsets will depend on accurate estimates of GHG emissions.

Previous studies have tested DNDC against field observations of (a) seasonal  $\text{CH}_4$  emissions from transplanted rice systems in India [Babu *et al.*, 2006; Pathak *et al.*, 2005], China, and Thailand [Li *et al.*, 2002; Cai *et al.*, 2003], as well as direct-seeded rice systems in Italy [Li *et al.*, 2002] and U.S. [Li, 2000; Li *et al.*, 2002], and (b) seasonal  $\text{N}_2\text{O}$  emissions from transplanted rice systems in India [Babu *et al.*, 2006; Pathak *et al.*, 2005] and China [Cai *et al.*, 2003]. The studies had varying levels of success and detail in the methods of calibration and validation. To the best of our knowledge, no model has been calibrated and validated for direct-seeded rice systems with different N fertilizer, establishment systems (water seeded and dry seeded), and fallow period straw and water management in the U.S.

The main objectives of this study were to calibrate and validate the DNDC model for California rice systems under varying management, soil environments, and weather conditions to predict seasonal and fallow period emissions of  $\text{CH}_4$  and  $\text{N}_2\text{O}$  at the site scale. We also sought to quantify the sensitivity of  $\text{CH}_4$  emissions to plant and soil properties (i.e., root to total plant biomass ratio,  $\text{N}_2$  fixation index, and soil bulk density) across water- and dry-seeded systems.

## 2. Materials and Methods

### 2.1. Description of DNDC Model

The DNDC model is a process-based model that predicts trace gas emissions (i.e.,  $\text{N}_2\text{O}$ ,  $\text{N}_2$ ,  $\text{NO}$ ,  $\text{NH}_3$ ,  $\text{CO}_2$ , and  $\text{CH}_4$ ) from soil under a variety of natural and managed ecosystems [e.g., Li, 2000; Zhang *et al.*, 2002a, 2002b; Stange *et al.*, 2000; Brown *et al.*, 2001]. The DNDC model is composed of the plant growth, soil climate, decomposition, nitrification, denitrification, and fermentation submodels and predicts C and N transformations at a daily time step. The crop growth, soil climate, and decomposition submodels interact and are driven by ecological (i.e., climate, soil, and crop) and management factors, which predicts the soil environmental variables (i.e., temperature, moisture level, pH, Eh, and substrate concentrations) that drive denitrification, nitrification, and fermentation processes. The soil climate and plant growth submodels predict soil temperature and

moisture level, while the decomposition and plant growth submodels predict concentrations of dissolved organic carbon (DOC) or other substrates ( $\text{NH}_4^+$ ,  $\text{NO}_3^-$ ,  $\text{CO}_2$ , and  $\text{H}_2$ ) through feedback from the microbe-oriented submodels. The modeled substrates play a key role in GHG production and consumption. A simple kinetic scheme called “anaerobic balloon” was developed in DNDC to link the substrate concentrations to GHG production [Li *et al.*, 2004; Li, 2007]. The size of the anaerobic balloon (or volumetric portion of anaerobic microsites) is determined by soil Eh, a function of concentrations of the substrates serving as electron donor (e.g., DOC and  $\text{H}_2$ ) or electron acceptor (e.g.,  $\text{O}_2$  and  $\text{NO}_3^-$ ). Based on thermodynamic theory of sequential reduction of oxidants according to their redox potential [Ponnamperuma, 1981; Zehnder and Stumm, 1988], each oxidant has its own anaerobic balloon whose size is driven by soil concentrations of  $\text{O}_2$ ,  $\text{NO}_3^-$ ,  $\text{Mn}^{4+}$ ,  $\text{Fe}^{3+}$ ,  $\text{SO}_4^{2-}$ , and  $\text{CO}_2$ , consecutively with decreasing soil Eh from 650 to  $-150$  mV.

The Nernst equation is used to estimate Eh:

$$\text{Eh} = E_0 - \frac{0.059}{n} \log\left(\frac{[\text{Rd}]}{[\text{Ox}]}\right) - \frac{0.059m}{n} \text{pH} \quad (1)$$

where Eh is soil redox potential (V),  $E_0$  is standard redox potential (V), [Rd] is concentration of reductive species of dominant oxidant ( $\text{mol L}^{-1}$ ), [Ox] is concentration of oxidative species of dominant oxidant ( $\text{mol L}^{-1}$ ),  $n$  is number of exchanged electrons, and  $m$  is number of exchanged protons. The modeled Eh determines the occurrence of oxidation-reduction reactions. When the soil Eh changes, the size of the anaerobic balloon will shrink or swell to allocate the relevant substrates inside and outside the balloon for anaerobic and aerobic processes, respectively.

As a common energy source for most microbes, DOC availability is important in controlling most of the microbe-mediated redox reactions in the soil. In DNDC, DOC is assumed to come from two sources, soil organic carbon (SOC) decomposition and root exudation, which are quantified with the decomposition submodel [Li *et al.*, 1992] and the plant growth submodel, respectively. The plant-derived DOC is empirically calculated as follows:

$$\text{DOC}_r = 0.001 (1 + \text{PGI}) R \quad (2)$$

where  $\text{DOC}_r$  is DOC produced from root exudation ( $\text{kg C ha}^{-1} \text{d}^{-1}$ ), PGI is plant growth index (0–1), and  $R$  is root biomass ( $\text{kg C ha}^{-1}$ ). In DNDC, DOC can be also produced from decomposition of SOC. The rate of decomposition of SOC is described by first-order kinetics for each of the SOC pools (i.e., plant residue, humads, and humus) in DNDC. Each SOC pool decomposes independently and is affected by soil clay content, C to N ratio of bulk soil organic matter, temperature, and moisture [Li *et al.*, 1992].

$$\Delta[\text{SOC}_i] = \mu_{\text{clay}} \mu_{\text{C:N}} \mu_{t,m} (S k_i) \quad (3)$$

where  $\Delta[\text{SOC}_i]$  is the decomposition rate of the sub-SOC pool  $i$  ( $\text{mol C m}^{-3} \text{s}^{-1}$ ),  $\mu_{\text{clay}}$  is the clay content reduction factor,  $\mu_{\text{C:N}}$  is the C to N ratio reduction factor,  $\mu_{t,m}$  is the combined temperature and moisture reduction factor,  $S$  is the organic C content in pool  $i$  ( $\text{mol C m}^{-3}$ ), and  $k_i$  is the specific decomposition rate of pool  $i$  ( $\text{s}^{-1}$ ).

In DNDC, the decomposed SOC is partitioned to microbial biomass and DOC based on the concept of microbial efficiency. The value of microbial efficiency adopted in DNDC is 0.2, which allocates 20% of the decomposed SOC to microbial biomass and 80% to the DOC pool. DOC is highly mobile in the soil profile as it can be utilized as an energy source by a wide range of microbes in soil and oxidized to  $\text{CO}_2$ . However, an instantaneous pool of DOC exists, whose size is determined by the balance between the production and consumption rates of DOC in the soil [Li *et al.*, 1992, 1994].

Under anaerobic conditions, fermentation and syntrophy of DOC lead to productions of acetate ( $\text{CH}_3\text{COO}^-$ ),  $\text{CO}_2$ , and  $\text{H}_2$ , which are three precursors of  $\text{CH}_4$  production. As DNDC does not simulate fermentation and syntrophy separately, the two phases are combined into one as anaerobic decomposition of DOC. First, DNDC calculates the rate of production of the monosaccharide portion of DOC, i.e., glucose ( $\text{C}_6\text{H}_{12}\text{O}_6$ ), using Michaleis-Menten kinetics:

$$\Delta[\text{C}_6\text{H}_{12}\text{O}_6] = \frac{V_{\text{max,DOC}} \cdot a[\text{DOC}]}{k_{\text{DOC}} + a[\text{DOC}]} \quad (4)$$

where  $\Delta[\text{C}_6\text{H}_{12}\text{O}_6]$  is the  $\text{C}_6\text{H}_{12}\text{O}_6$  production rate from anaerobic decomposition of DOC ( $\text{mol C m}^{-3} \text{s}^{-1}$ ),  $V_{\text{max,DOC}}$  is the maximum rate of anaerobic decomposition of DOC,  $a$  is the monosaccharide fraction of DOC,  $a$  is the monosaccharide fraction of the DOC pool,  $[\text{DOC}]$  is the concentration of DOC in the soil pore water ( $\text{mol C m}^{-3}$ ), and  $k_{\text{DOC}}$  is the concentration of DOC at half of the maximum rate of anaerobic decomposition of DOC ( $\text{mol C m}^{-3}$ ). Second, it is assumed that the fraction of  $\text{C}_6\text{H}_{12}\text{O}_6$  to total DOC is constant, and based on a generalized reaction of anaerobic decomposition of  $\text{C}_6\text{H}_{12}\text{O}_6$ , rates of production of  $\text{CH}_3\text{COO}^-$  ( $\text{mol C m}^{-3} \text{s}^{-1}$ ),  $\text{CO}_2$  ( $\text{mol C m}^{-3} \text{s}^{-1}$ ), and  $\text{H}_2$  ( $\text{mol H m}^{-3} \text{s}^{-1}$ ) are calculated as 2, 2, and 4 times the rate of production of  $\text{C}_6\text{H}_{12}\text{O}_6$ , respectively.

Another source of  $\text{CO}_2$  is from plant root respiration, which is empirically calculated as follows:

$$\text{CO}_2 \text{ root} = 0.025 R F_{\text{age}} \quad (5)$$

$$F_{\text{age}} = -2.8348 \text{ PGI}^2 + 2.4848 \text{ PGI} + 0.4554 \quad (6)$$

where  $\text{CO}_2 \text{ root}$  is  $\text{CO}_2$  production derived from root respiration ( $\text{kg C ha}^{-1} \text{d}^{-1}$ ),  $R$  is plant root biomass ( $\text{kg C ha}^{-1}$ ), and  $F_{\text{age}}$  is the effect of plant growth stage.

In DNDC,  $\text{CH}_4$  is produced through acetotrophic or hydrogenotrophic methanogenesis. The Michaelis-Menten equation is utilized in DNDC to calculate the rates of these two  $\text{CH}_4$ -producing reactions, as follows:

$$V_{\text{CH}_4-a} = \frac{V_{\text{max}-a} [\text{CH}_3\text{COOH}^-]}{k_{\text{ma}} + [\text{CH}_3\text{COOH}^-]} \quad (7)$$

where  $V_{\text{CH}_4-a}$  is  $\text{CH}_4$  production rate from acetotrophic methanogenesis ( $\text{mol m}^{-3} \text{s}^{-1}$ ),  $V_{\text{max}-a}$  is maximum  $\text{CH}_4$  production rate from acetotrophic methanogenesis ( $\text{mol m}^{-3} \text{s}^{-1}$ ), and  $k_{\text{ma}}$  is the concentration of acetate,  $[\text{CH}_3\text{COO}^-]$ , at a half of the maximum  $\text{CH}_4$  production rate ( $\text{mol m}^{-3} \text{s}^{-1}$ ). Based on *Van Bodegom and Scholten* [2001], the value of  $V_{\text{max}-a}$  is  $0.00002 \text{ mol m}^{-3} \text{s}^{-1}$  and  $k_{\text{ma}}$  is  $2.56 \text{ mol m}^{-3} \text{s}^{-1}$  at  $30^\circ\text{C}$ .  $V_{\text{max}-a}$  is sensitive to temperature with  $Q_{10}=4.6$ , and

$$V_{\text{CH}_4-b} = \frac{V_{\text{max}-b} [\text{CO}_2]}{(k_{\text{mb}1} + [\text{CO}_2]) [\text{H}_2]} \quad (8)$$

where  $V_{\text{CH}_4-b}$  is  $\text{CH}_4$  production rate from hydrogenotrophic methanogenesis ( $\text{mol m}^{-3} \text{s}^{-1}$ ),  $V_{\text{max}-b}$  is maximum  $\text{CH}_4$  production rate from hydrogenotrophic methanogenesis ( $\text{mol m}^{-3} \text{s}^{-1}$ ),  $k_{\text{mb}1}$  and  $k_{\text{mb}2}$  are the concentrations of  $\text{CO}_2$  and  $\text{H}_2$ , respectively, at half of the maximum  $\text{CH}_4$  production rate ( $\text{mol m}^{-3} \text{s}^{-1}$ ), and  $[\text{CO}_2]$  and  $[\text{H}_2]$  are  $\text{CO}_2$  and  $\text{H}_2$  concentrations ( $\text{mol m}^{-3} \text{s}^{-1}$ ), respectively. Due to lack of experimental data to differentiate the constants  $V_{\text{max}}$  and  $k_{\text{ma}}$  by methanogenesis pathway in the aforementioned equations, the same constant values are used in both equations. Lastly, total daily  $\text{CH}_4$  production rates are calculated by summing the acetate-induced and  $\text{H}_2$ -induced  $\text{CH}_4$  production rates.

The total  $\text{CH}_4$  in each soil layer that is allocated to outside of the anaerobic balloon will be oxidized at the rate calculated as follows:

$$V_{\text{CH}_4-\text{O}} = \frac{V_{\text{CH}_4-\text{O-max}} [\text{CH}_4]}{k_{\text{mc}} + [\text{CH}_4]} \quad (9)$$

where  $V_{\text{CH}_4-\text{O}}$  is  $\text{CH}_4$  oxidation rate ( $\text{mol m}^{-3} \text{s}^{-1}$ ),  $V_{\text{CH}_4-\text{O-max}}$  is maximum  $\text{CH}_4$  oxidation rate ( $0.0001 \text{ mol m}^{-3} \text{s}^{-1}$ ),  $k_{\text{mc}}$  is the concentration of  $\text{CH}_4$  at a half of the maximum  $\text{CH}_4$  oxidation rate ( $0.008 \text{ mol m}^{-3} \text{s}^{-1}$ ), and  $[\text{CH}_4]$  is  $\text{CH}_4$  concentration ( $\text{mol m}^{-3} \text{s}^{-1}$ ).

The  $\text{CH}_4$  produced in the anaerobic soil profile can be transported to the atmosphere through three channels: diffusion, ebullition, and plant vascular transport. Diffusion of  $\text{CH}_4$  in the soil liquid phase across the simulated soil layers is driven by the  $\text{CH}_4$  concentration gradient between the layers and calculated as

$$dDF_i = F_d ([\text{CH}_4(i)] - [\text{CH}_4(i-1)]) \quad (10)$$

$$F_d = \frac{0.5}{1 + \text{clay}} \quad (11)$$

where  $dDF_i$  is  $\text{CH}_4$  diffusion rate in layer  $i$  ( $\text{mol m}^{-3} \text{s}^{-1}$ ),  $F_d$  is diffusion coefficient ( $\text{s}^{-1}$ ) which is a function of the fractional soil clay content, and  $[\text{CH}_4(i)]$  and  $[\text{CH}_4(i-1)]$  are  $\text{CH}_4$  concentrations ( $\text{mol C m}^{-3}$ ) in layer  $i$  and  $i-1$ ,

respectively. If the soil water is oversaturated with CH<sub>4</sub>, the excess CH<sub>4</sub> can escape from the soil profile to air by ebullition,

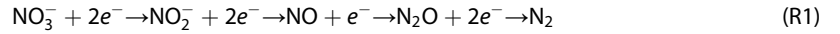
$$\text{CH}_{4\text{st}} = 5.357 (0.0285 e^{-0.0414 T} + 0.0115) \quad (12)$$

where CH<sub>4st</sub> is the CH<sub>4</sub> saturation concentration in water (kg C m<sup>-3</sup>) and *T* is soil temperature (°C). Note that ebullition is assumed to be independent from soil texture. Hydrophytes possess vascular structure that constitute a channel for CH<sub>4</sub> in the soil profile to escape to the atmosphere,

$$\text{FLUX}_{\text{pl}} = \frac{[\text{CH}_4] R}{(50 + R) V_{\text{as}}} \quad (13)$$

where FLUX<sub>pl</sub> is CH<sub>4</sub> flux through plant transport (kg C ha<sup>-1</sup> d<sup>-1</sup>), [CH<sub>4</sub>] is CH<sub>4</sub> concentration in soil (kg C ha<sup>-1</sup>), *R* is plant root biomass (kg C ha<sup>-1</sup>), and *V*<sub>as</sub> is plant vascularity index (0–1). Thus, daily total CH<sub>4</sub> emission is the sum of the CH<sub>4</sub> emitted through diffusion, ebullition, and plant-mediated transport.

N<sub>2</sub>O is an intermediate of denitrification or nitrification reactions depending on the soil Eh. DNDC simulates the sequential reactions of denitrification from nitrate (NO<sub>3</sub><sup>-</sup>) to N<sub>2</sub> gas.



The rate of each step of denitrification is a function of the growth rate of the respective denitrifier population. The denitrifier growth dynamics are calculated in the following order of steps based on the Michaelis-Menten kinetics:

$$u_{\text{NO}_3} = u_{\text{NO}_3, \text{max}} \left( \frac{[\text{DOC}]}{k_c + [\text{DOC}]} \right) \left( \frac{[\text{NO}_3]}{k_n + [\text{NO}_3]} \right) \quad (14)$$

$$u_{\text{NO}_2} = u_{\text{NO}_2, \text{max}} \left( \frac{[\text{DOC}]}{k_c + [\text{DOC}]} \right) \left( \frac{[\text{NO}_2]}{k_n + [\text{NO}_2]} \right) \quad (15)$$

$$u_{\text{NO}} = u_{\text{NO}, \text{max}} \left( \frac{[\text{DOC}]}{k_c + [\text{DOC}]} \right) \left( \frac{[\text{NO}]}{k_n + [\text{NO}]} \right) \quad (16)$$

$$u_{\text{N}_2\text{O}} = u_{\text{N}_2\text{O}, \text{max}} \left( \frac{[\text{DOC}]}{k_c + [\text{DOC}]} \right) \left( \frac{[\text{N}_2\text{O}]}{k_n + [\text{N}_2\text{O}]} \right) \quad (17)$$

where *u*<sub>NO<sub>3</sub></sub>, *u*<sub>NO<sub>2</sub></sub>, *u*<sub>NO</sub>, and *u*<sub>N<sub>2</sub>O</sub> are relative growth rates of NO<sub>3</sub><sup>-</sup>, NO<sub>2</sub><sup>-</sup>, NO, and N<sub>2</sub>O denitrifiers, respectively (kg C m<sup>-3</sup> h<sup>-1</sup>); *u*<sub>NO<sub>3</sub>,max</sub>, *u*<sub>NO<sub>2</sub>,max</sub>, *u*<sub>NO,max</sub>, and *u*<sub>N<sub>2</sub>O,max</sub> are the maximum relative growth rates of NO<sub>3</sub><sup>-</sup>, NO<sub>2</sub><sup>-</sup>, NO, and N<sub>2</sub>O denitrifiers, respectively, fixed as 0.067, 0.67, 0.34, and 0.34 kg C m<sup>-3</sup> h<sup>-1</sup>, respectively; [DOC] is DOC concentration in the anaerobic balloon (kg C m<sup>-3</sup>); [NO<sub>3</sub>], [NO<sub>2</sub>], [NO] and [N<sub>2</sub>O] are concentrations of NO<sub>3</sub><sup>-</sup>, NO<sub>2</sub><sup>-</sup>, NO, and N<sub>2</sub>O in the anaerobic balloon (kg N m<sup>-3</sup>); and *k*<sub>c</sub> and *k*<sub>n</sub> are half-saturation values of soluble carbon (0.017 kg C m<sup>-3</sup>) and N oxides (0.083 kg N m<sup>-3</sup>), respectively. The total growth rate (*u*<sub>DN</sub>, kg C m<sup>-3</sup> h<sup>-1</sup>) of denitrifiers is calculated as

$$u_{\text{DN}} = u_{\text{NO}_3} F_{\text{pH-NO}_3} + u_{\text{NO}_2} F_{\text{pH-NO}_2} + u_{\text{NO}} F_{\text{pH-NO}} + u_{\text{N}_2\text{O}} F_{\text{pH-N}_2\text{O}} \quad (18)$$

where *F*<sub>pH-NO<sub>3</sub></sub>, *F*<sub>pH-NO<sub>2</sub></sub>, *F*<sub>pH-NO</sub>, and *F*<sub>pH-N<sub>2</sub>O</sub> are factors accounting for soil pH effects on relative growth rates of NO<sub>3</sub><sup>-</sup>, NO<sub>2</sub><sup>-</sup>, NO, and N<sub>2</sub>O denitrifiers, respectively:

$$F_{\text{pH-NO}_3} = 1 - \left( 1 + e^{((\text{pH}-4.25)/0.5)} \right)^{-1} \quad (19)$$

$$F_{\text{pH-NO}_2} = 1 - \left( 1 + e^{((\text{pH}-4.25)/0.5)} \right)^{-1} \quad (20)$$

$$F_{\text{pH-NO}} = 1 - \left( 1 + e^{(\text{pH}-5.25)} \right)^{-1} \quad (21)$$

$$F_{\text{pH-N}_2\text{O}} = 1 - \left( 1 + e^{((\text{pH}-6.25)/1.5)} \right)^{-1} \quad (22)$$

Death rate of denitrifiers is calculated as

$$(dB/dt)_d = M_c Y_c B(t) \quad (23)$$

where (*dB/dt*)<sub>d</sub> is death rate of denitrifiers (kg C m<sup>-3</sup> h<sup>-1</sup>), *M*<sub>c</sub> is maintenance coefficient of denitrifiers (kg C/kg C/h), *Y*<sub>c</sub> is DOC released from death of denitrifiers (kg C/kg C), and *B*(*t*) is biomass of

denitrifiers at time  $t$  ( $\text{kg C m}^{-3}$ ). By tracking the growth and death rates of the four groups of denitrifiers, DNDC calculates production and consumption of  $\text{NO}_3^-$ ,  $\text{NO}_2^-$ ,  $\text{NO}$ ,  $\text{N}_2\text{O}$ , and  $\text{N}_2$  at an hourly time step.

DNDC calculates production of  $\text{N}_2\text{O}$  from nitrification as

$$\text{N}_2\text{O}_N = 0.0006 R_N \text{ wfps } F_T \quad (24)$$

$$F_T = \frac{T - 9}{20} \quad (25)$$

where  $\text{N}_2\text{O}_N$  is nitrification-induced  $\text{N}_2\text{O}$  production ( $\text{kg N}_2\text{O-N ha}^{-1} \text{ d}^{-1}$ ),  $R_N$  is nitrification rate ( $\text{kg N ha}^{-1} \text{ d}^{-1}$ ),  $\text{wfps}$  is the fraction of water-filled pore space, and  $F_T$  is the effect of temperature ( $^{\circ}\text{C}$ ). The  $R_N$  is a function of concentration of ammonium ( $\text{kg N ha}^{-1}$ ), biomass of nitrifiers ( $\text{kg C ha}^{-1}$ ), and soil pH, which limit maximum nitrification rate.

Daily  $\text{N}_2\text{O}$  production is the sum of the modeled daily  $\text{N}_2\text{O}$  production from denitrification and nitrification. Daily  $\text{N}_2\text{O}$  emission is calculated with a simplified gas diffusion routine empirically developed in DNDC:

$$\text{N}_2\text{O}_E = 30 \left( 0.0006 + \frac{0.0013 \text{ clay}}{0.315} \right) + \left( 0.013 - \frac{0.005 \text{ clay}}{0.315} \right) 2^{\frac{T}{20}} \text{ PORO} \quad (26)$$

where  $\text{N}_2\text{O}_E$  is  $\text{N}_2\text{O}$  emission rate ( $\text{kg N}_2\text{O-N ha}^{-1} \text{ d}^{-1}$ ),  $\text{clay}$  is fractional soil clay content,  $T$  is soil temperature ( $^{\circ}\text{C}$ ), and  $\text{PORO}$  is soil porosity.

Model inputs include daily climate (e.g., air temperature, precipitation, wind speed, solar radiation, and humidity), soil physical and chemical properties (e.g., texture, bulk density, hydraulic conductivity, pH, soil organic C content and C:N ratio, and mineral N content), and crop parameters (e.g., plant biomass fractions and C:N ratios of grain, leaf, stem, and root; maximum yield; thermal degree days to maturity; optimum temperature; and nitrogen fixation index) and management schedules (e.g., dates of seeding, harvest, tillage, irrigation, and fertilizer application).

## 2.2. Site Descriptions

Here we synthesized all of the published data available in California rice systems for which adequate input data are available for site-level modeling. The data used to calibrate and validate the DNDC model came from eight field experiments (designated F1, F2, F3, F4, F5, F6, F7, and F8) distributed throughout the Sacramento Valley of California in the U.S. (Figure 1). The California rice-growing region is characterized by a Mediterranean climate with hot summers and the majority of rainfall occurring in winter months. Measured soil properties are summarized in Table 1. Default soil hydraulic input parameters were set based on soil texture, as they were not measured at any of the sites. Detailed management routines were obtained from the publications, directly from the authors, and/or estimated based on conventional management practices and weather data for that location. Experimental treatments and field management are described in Table 2. Key crop information obtained from each site included cultivar type, seeding and harvest dates, N fertilizer input, and fraction of straw left in the field after harvest. Depending on the cultivar grown, a specific set of crop input parameters was determined and further adjusted through the model calibration (Table 3). Detailed management routines, including dates and methods of tillage, irrigation, and fertilizer application, were also obtained. Additional details of the experiments can be found in their respective publications [Lauren *et al.*, 1994; Bossio *et al.*, 1999; Fitzgerald *et al.*, 2000; Adviento-Borbe *et al.*, 2013; Pittelkow *et al.*, 2013, 2014b; Simmonds *et al.*, 2015]. Briefly, the data represented a range of N fertilizer rates (i.e., 0 to  $260 \text{ kg N ha}^{-1}$ ) and seeding systems (i.e., water seeded or dry seeded), with distinct fallow period straw and water management regimes (i.e., straw burning, straw incorporation, and with and without flooding).

## 2.3. Model Calibration

DNDC was calibrated for a high-yielding, semidwarf rice cultivar (M206) and a traditional cultivar (Koshihikari) using field-based measurements of grain, stem, leaf, and root biomass, and corresponding C to N ratios. Plant samples were collected from four field experiments (five site-year combinations) [Adviento-Borbe *et al.*, 2013; Pittelkow *et al.*, 2013; Simmonds *et al.*, 2015] and are summarized in Table 3. The data were used for the calibration of two unique sets of cultivar-specific input parameters in the crop growth submodel. The model was constrained using these measurements within 1 standard deviation (SD) of the pooled average of two field experiments planted to M206 (three site-year combinations) and three field experiments planted to

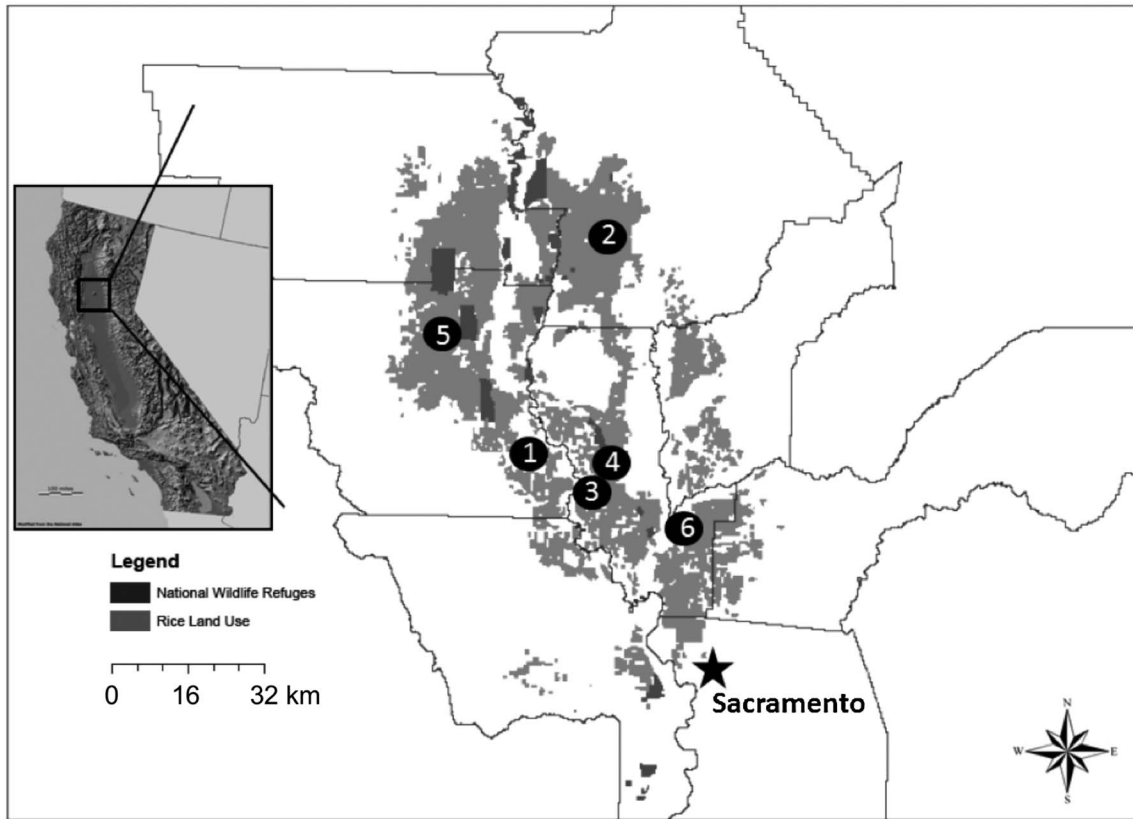


**Figure 1.** California map showing the rice-growing region in the Sacramento Valley and the location of the eight study sites (Table 1), represented by the numbered circles: (1) Arbuckle (F1), (2) Biggs (F2 and F3), (3) Robbins (F4), (4) Robbins (F5), (5) Maxwell (F6 and F7), and (6) Pleasant Grove (F8). The California State Capitol, Sacramento, is indicated by the star.

**Table 1.** Soil Properties at Eight Study Sites (Designated F1–F8) in California, USA, Used for Model Calibration and/or Validation

Study Site	Taxonomic Classification	Bulk Density (g cm <sup>-3</sup> )	Clay (%)	Texture	Soil Organic Carbon (%)	Total N (%)	pH	Source
Arbuckle (F1)	Fine, smectitic, thermic Xeric Endoaquerts	1.03	57	Clay	1.69 <sup>1</sup>	0.14	6.0 <sup>a</sup>	<i>Pittelkow et al. [2013]</i>
Biggs (F2)	Fine, smectitic, thermic Xeric Epiaquerts and Duraquerts	1.02	45	Clay loam <sup>b</sup>	1.50 <sup>1</sup>	0.08	5.5 <sup>a,b</sup> , 5.9 <sup>a,c</sup>	<i>Pittelkow et al. [2014b]</i>
Biggs (F3 <sup>d</sup> )	Fine, smectitic, thermic Xeric Epiaquerts and Duraquerts	1.13	47	Clay	1.26	0.08	4.8	<i>Simmonds et al. [2015]</i>
Robbins (F4)	Fine, smectitic, thermic Xeric Endoaquert	0.95	59	Clay	1.34	0.14	6.1	<i>Adviento-Borbe et al. [2013]</i>
Robbins (F5)	Fine, smectitic, thermic Typic Argixerolls	1.53	28	Loam	1.37	0.11	5.5	<i>Adviento-Borbe et al. [2013]</i>
Maxwell (F6)	Fine, montmorillonitic, thermic, Typic Pelloxerert	0.76 <sup>e</sup>	50	Silty clay	1.96	0.17 <sup>f</sup> , 0.16 <sup>g</sup>	6.9	<i>Bossio et al. [1999]</i>
Maxwell (F7)	Thermic Sodic Endoaquert	0.76 <sup>e</sup>	50	Silty clay	1.74	0.16	6.6	<i>Fitzgerald et al. [2000]</i>
Pleasant Grove (F8)	Fine loamy, mixed, thermic Fluventic Haploxeroll	1.20 <sup>h</sup>	23	Loam	1.07	0.09	4.8	<i>Lauren et al. [1994]</i>

<sup>a</sup>Differs from published values based on additional available data.

<sup>b</sup>Stale seedbed treatments.

<sup>c</sup>Conventional tillage treatment.

<sup>d</sup>Calibration only.

<sup>e</sup>Estimate based on data from *Bird [2001]* and *Bossio et al. [1999]*.

<sup>f</sup>Straw incorporated treatment.

<sup>g</sup>Straw burned treatment.

<sup>h</sup>Estimate based on soil texture.

**Table 2.** Summary of Field Management Practices at Eight Study Sites (Table 1)<sup>a</sup>

Study Site	Years Simulated	Cultivar Grown	Seeding System	Fertilizer N Rates (kg N ha <sup>-1</sup> )	Fallow Period Management	
					Water	Straw
F1	2009–2012 <sup>b</sup>	M206	Water seeded	1. 0N 2. 80N 3. 140N <sup>e</sup> 4. 200N <sup>f</sup> 5. 260N	FF <sup>c</sup>	SI <sup>d</sup>
F2	2008–2009	M206	1. WSCON <sup>g</sup> 2. WSSSB <sup>h</sup> 3. DSSSB <sup>i</sup>	168	FF	SI
F3	2011	1. M206 <sup>e</sup> 2. KOSH <sup>e</sup>	Water seeded	130	NFF <sup>j</sup>	SB <sup>k</sup>
F4	2010–2011	KOSH	Dry seeded	1. 0N 2. 50N 3. 100N <sup>e</sup> 4. 150N 5. 200N	NFF	SI
F5	2010–2012 <sup>l</sup>	KOSH	Dry seeded	1. 0N 2. 50N 3. 100N <sup>e</sup> 4. 150N 5. 200N	FF	SI
F6	1996–1997 <sup>l</sup>	M202	Water seeded	159, 167		1. FF and SI 2. FF and SB
F7	1994–1996 <sup>l</sup>	M202	Water seeded	181, 173, 159		1. FF and SI 2. FF and SB 3. NFF and SI
F8	1991–1992 <sup>l</sup>	M202	Water seeded	100		1. FF and SB 2. FF and SI

<sup>a</sup>Main management treatments are indicated by a numbered list.

<sup>b</sup>First year is used as “spin-up,” and two different simulations were used for 2010 and 2011 due to different fertilizer histories.

<sup>c</sup>Fallow period flood.

<sup>d</sup>Straw incorporated.

<sup>e</sup>Used in calibration only.

<sup>f</sup>Second year used in calibration.

<sup>g</sup>Water seeded and conventional tillage.

<sup>h</sup>Water seeded and stale seedbed.

<sup>i</sup>Dry seeded and stale seedbed.

<sup>j</sup>No fallow period flood.

<sup>k</sup>Straw burned.

<sup>l</sup>First year used as spin-up to account for winter flooding and/or straw or water management treatments prior to the start of the growing season.

Koshihikari (three site-year combinations) (Table 3). A similar cultivar to M206 (i.e., M202) was grown at three of the sites used in the model validation (Table 2). For these sites a modified version of the M206 calibration was used (Table 3). While aboveground biomass data were based on samples collected at harvest, root samples were collected immediately prior to field drainage, which was between 115 days and 132 days after seeding, depending on the location. We assumed that root biomass declined by 25% due to root senescence during the period from drainage to harvest (18 to 42 days after drainage), which is within the range of root biomass decay from the ripening stage to harvest reported by *Baruah et al.* [2010] for both traditional and high-yielding varieties. Additionally, grain, leaf, and stem ratios were adjusted to reflect observed pooled mean harvest index across sites.

An iterative approach was used to tune the crop input parameters that were not measured (i.e., maximum grain yield, optimal temperature, and thermal degree days to maturity). Once all site-specific climate, soil, and management details (seeding, harvest, tillage, fertilization, and flooding), as well as the measured cultivar-specific crop parameters, were set in the model, optimal temperature and thermal degree days to maturity were each set to a single value for M206 and Koshihikari that optimized agreement between observed and simulated yield across all site-treatment combinations designated for calibration (Table 2). Thus, the two sets of cultivar-specific crop parameters were calibrated in this study. The maximum C yield

**Table 3.** Crop Input Parameters Calibrated for Two Rice Cultivars, M206 and Koshihikari

	Biomass Ratio						C:N Ratio						Maximum Demand (kg N ha <sup>-1</sup> )	TDD <sup>b</sup>	T <sub>c</sub> (°C)	N Fixation Index (kg Crop N kg <sup>-1</sup> Soil N)
	Grain (N <sup>a</sup> =6)	Leaf (N=3)	Stem (N=3)	Root (N=6)	Grain (N=12)	Leaf (N=3)	Stem (N=3)	Root (N=6)	Maximum Yield (Mg C ha <sup>-1</sup> )	Root (N=6)	Stem (N=3)	Leaf (N=3)				
M206 <sup>d</sup>	0.45	0.13	0.33	0.09	40	42	78	43	5.00	230	3200	27	1.18			
Koshihikari	0.41	0.125	0.375	0.09	40	44	79	49	4.20	202	3200	27	1.18			
Default	0.41	0.27	0.27	0.05	45	85	85	85	3.38		2000	25	1.05			

<sup>a</sup>Sample size of observed field data for each cultivar.

<sup>b</sup>Total degree days to maturity.

<sup>c</sup>Optimum temperature for plant growth.

<sup>d</sup>At the sites where M202 cultivar was grown (Table 2), maximum yield was set to 4768 kg C ha<sup>-1</sup> and N demand to 219 kg N ha<sup>-1</sup> based on a reported 4.65% lower yield on average for M202 than M206 (California Cooperative Rice Research Foundation's 2004 and 2006 Annual Reports on Statewide and Rice Experiment Station yield tests).

parameters determined for M206 and Koshihikari cultivars were similar to average maximum yields reported by Pittelkow *et al.* [2013] and Simmonds *et al.* [2013] for M206 (i.e., 4.5 Mg C ha<sup>-1</sup> and 5.8 Mg C ha<sup>-1</sup>, respectively) and by Adviento-Borbe *et al.* [2013] and Horie *et al.* [1997] for Koshihikari (i.e., 3.6 Mg C ha<sup>-1</sup> and 4.6 Mg C ha<sup>-1</sup>, respectively).

The N<sub>2</sub> fixation index, water demand, and vascularity are additional input parameters in the crop growth submodel. Default values were used for water demand (508 g H<sub>2</sub>O g<sup>-1</sup> dry matter) and vascularity (1) of the rice plant. The N<sub>2</sub> fixation index indicates the proportion of total plant N derived from biological N<sub>2</sub> fixation. However, we set it to 1.18 kg plant N kg<sup>-1</sup> of soil N to simulate additional N inputs from nonsymbiotic N<sub>2</sub> fixation. This value resulted in annual soil N<sub>2</sub> fixation values ranging from 17 to 20 kg N ha<sup>-1</sup> yr<sup>-1</sup> across the calibration data set, which is within the range estimated for nonsymbiotic N<sub>2</sub> fixation in a long-term N balance experiment in irrigated rice systems fertilized with urea-N (i.e., 13 kg N ha<sup>-1</sup> crop<sup>-1</sup> to 36 kg N ha<sup>-1</sup> crop<sup>-1</sup>) [Ladha *et al.*, 2000].

Daily weather data, including maximum and minimum air temperature, precipitation, wind speed, radiation, and humidity, were obtained from the California Irrigation Management Information System database (cimis.water.ca.gov) using the closest weather station to each study site with the most complete data set. Annual precipitation-weighted N concentrations (NH<sub>4</sub><sup>+</sup> + NO<sub>3</sub><sup>-</sup>) in rainfall were obtained from the National Trends Network of the National Atmospheric Deposition Program (nadp.sws.uiuc.edu), using the station located in Yolo County, California. In the case of the atmospheric background NH<sub>3</sub> concentration parameter, the default value (0.06 μg N m<sup>-3</sup>) was used for all study sites.

Soil input parameters were modified for each study site and included soil bulk density, clay content, texture, pH, organic carbon, nitrate, ammonium, and carbon to nitrogen ratio of soil organic matter. These data were obtained from the published literature for each experiment or from personal communications, including replicate observations (Table 1). DNDC default values for soil NO<sub>3</sub><sup>-</sup> and NH<sub>4</sub><sup>+</sup> concentrations (0.5 mg kg<sup>-1</sup> and 0.05 mg kg<sup>-1</sup>, respectively) were used at F5–F8 due to unavailability of data.

Site-specific management input parameters were used and included timing of seeding and harvest and fraction of straw left in the field postharvest; timing and depth of tillage; timing, type, and depth of fertilizer application; and dates of flooding and draining using the conventional 10 cm surface water depth option. These data were obtained from the published literature for each experiment or through personal communications. In the case that detailed management events were not available, management input parameters were estimated based on a combination of considerations: knowledge of the field

site, including daily weather and historic management practices, and recommendations for the region and the type of seeding system (<http://coststudies.ucdavis.edu>).

#### 2.4. Model Validation and Performance Tests

Major model modifications related to crop growth and CH<sub>4</sub> production and oxidation have been made in recent years. All the internal parameters were fixed without any changes during the applications of DNDC for this study. The calibrations conducted in this study only focused on the external parameters such as crop parameters or soil properties. Unless otherwise noted, all results and discussion of observations and model performance exclude the calibration data points. The validation data set we used represents seven fields (nine site-year combinations) distributed across the major rice-growing region in California. We estimated cumulative seasonal and fallow period emissions using linear interpolation of the daily fluxes. Thus, depending on the exact range of dates used in the calculations, our cumulative flux values may differ slightly from the published values. We evaluated the predictive ability of the DNDC model for estimating grain yield of the selected two cultivars (M206 and Koshihikari) and seasonal and fallow period CH<sub>4</sub> and N<sub>2</sub>O emissions. We determined the mean squared deviation (MSD) between modeled and observed values and partitioned it into three distinct and meaningful components: lack of correlation, nonunity slope, and squared bias [Gauch *et al.*, 2003]:

$$\text{MSD} = \frac{\sum (X_n - Y_n)^2}{N} \quad (27)$$

$$\text{RMSD} = \sqrt{\text{MSD}} \quad (28)$$

where RMSD is the root-mean-square deviation,  $X$  and  $Y$  are simulated and observed values, respectively,  $N$  = number of observations, and  $n = 1, 2, \dots, N$ .

Sensitivity analyses were performed for CH<sub>4</sub> emissions only, due to the relative importance of CH<sub>4</sub> to net soil GWP in rice systems and to the poor validation of N<sub>2</sub>O emissions. The sensitivity of model predictions of seasonal CH<sub>4</sub> emissions to soil bulk density, root to total plant biomass ratio, and the N<sub>2</sub> fixation parameter were evaluated at one of the field sites where several seeding systems were tested (water-seeded conventional, dry-seeded stale seedbed, and water-seeded stale seedbed) [Pittelkow *et al.*, 2014b] (Tables 1 and 2). These parameters were chosen based on the uncertainty and/or variability of their values in cultivated agricultural soils. The range of potential parameter values for soil bulk density [Bossio *et al.*, 1999; Adviento-Borbe *et al.*, 2013] and root to total plant biomass ratio [Bossio *et al.*, 1999; Simmonds *et al.*, 2015] were set based on the measured range of their values in California paddy soils, which in some cases included  $-1$  SD of mean measured values. Due to lack of data from U.S. rice systems, the range of potential parameter values used for the N<sub>2</sub> fixation index was based on studies in Asia under a variety of fertility treatments [Peoples and Craswell, 1992; Ladha *et al.*, 2000].

### 3. Results

#### 3.1. Crop Growth Simulation

Differences in modeled and observed total plant N in biomass of Koshihikari and M206 were within 59 kg N ha<sup>-1</sup> throughout the growing season across all calibration plots at F1, F3, and F5 in 2011 (Figure 2). Accumulation of C and N in root tissue over time followed the observed seasonal patterns with most predictions within < 30% of measurements (Figure 3). However, simulated root C at midtillering was overestimated at all sites by 33% to 184%, but model predictions improved after this (Figure 3). Simulated straw (leaf + stem) N deviated from measurements by 26% on average across all sites with the greatest overestimation at midtillering (Figure 3). The greatest discrepancy in simulated plant C dynamics was in accumulation of C in straw biomass, which was overestimated from midtillering to heading in all cases. However, simulated straw C improved later in the season with 31% average absolute relative deviation across all sites at field drainage and maturity. Modeled C accumulation in grain started within 13 days to 32 days prior to the observed heading dates across all sites (Figure 3) (heading dates not shown for F1 or F5). Grain C at harvest was predicted well for Koshihikari at F5 and M206 at both F1 and F3 (<8.2% absolute relative deviation), but the model overestimated grain C for Koshihikari at F3 by about 1.1 Mg C ha<sup>-1</sup>.

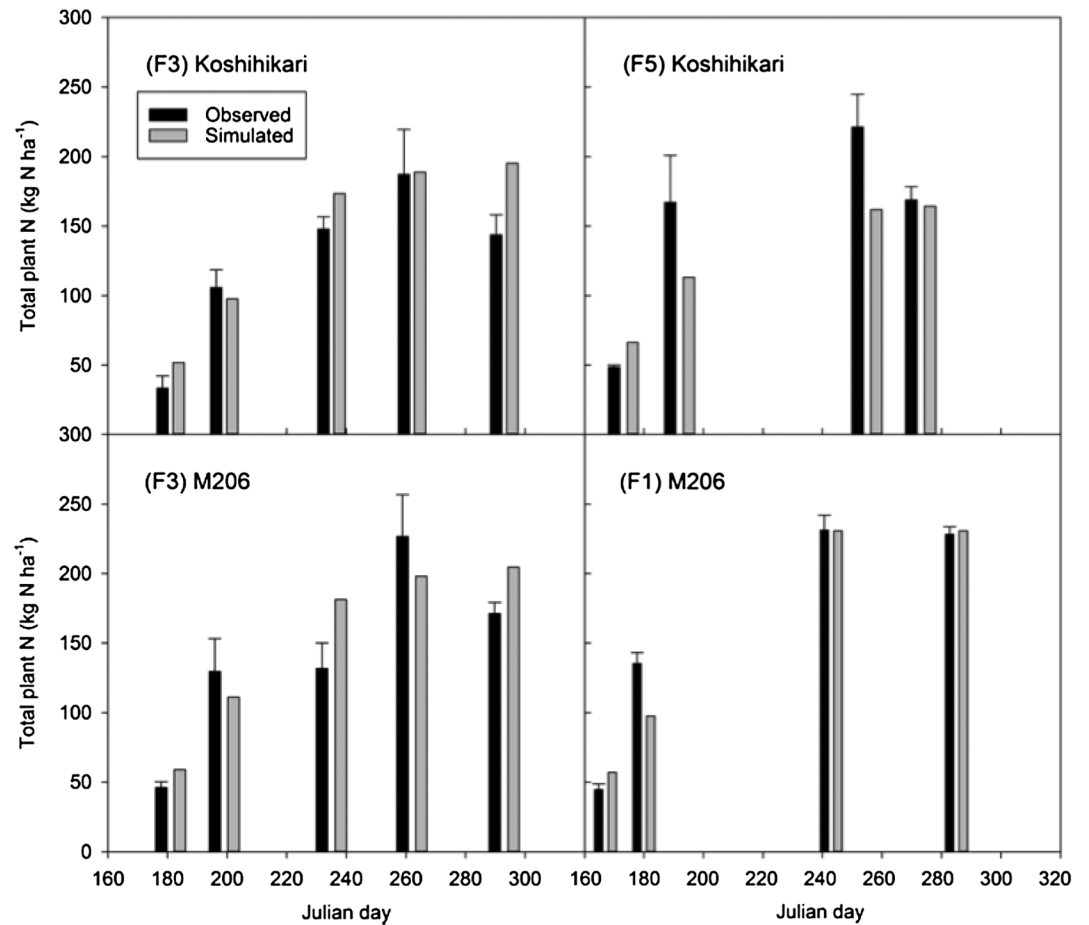


**Figure 2.** Calibrated and observed seasonal changes in total plant N (aboveground and belowground) in (top row) Koshihikari and (bottom row) M206 at F1, F3, and F5 in 2011. Error bars represent the standard error of three replicates. Sampling dates correspond to (first to last) midtillering, panicle initiation, heading, field drainage, and maturity, except at F1 and F5 where there was no measurement at heading. Note that these data are from the calibration data set, and the root portion of the final total plant N observation is extrapolated from the previous measurement at drainage.

Observed yields in the validation data set ranged from 1.4 to 5.0 Mg C ha<sup>-1</sup> across management treatments and sites (Figure 4). On average, yield predictions for each treatment had an absolute relative deviation of 19.8%. For M206 and Koshihikari, the model was able to simulate 30% and 78% of observed variation in yields, respectively, with an RMSD of 0.90 Mg C ha<sup>-1</sup> (N = 14) and 0.69 Mg C ha<sup>-1</sup> (N = 8), respectively (Figure 4). The greatest proportion (70.4%) of variance was due to lack of correlation (80.5%) for M206 and to nonunity slope (69.6%) for Koshihikari. The discrepancy between simulated and observed was generally greater at higher observed yield levels, with the majority of predictions overestimating yield, particularly for Koshihikari. While yield predictions at F1, F4, F5, and F8 were not biased to overestimate or underestimate across all treatments, yield at F6 was underestimated and F2 was overestimated in all cases (Figure 4).

**3.2. Methane Emissions**

While there was poor correlation between observed and modeled fallow period CH<sub>4</sub> emissions (R<sup>2</sup> = 0.13; RMSD = 31.1 kg CH<sub>4</sub>-C ha<sup>-1</sup>), the model predicted growing season CH<sub>4</sub> emissions reasonably well (R<sup>2</sup> = 0.85; RMSD = 66.8 kg CH<sub>4</sub>-C ha<sup>-1</sup>) across seven study sites (N = 28) with both water- and dry-seeded systems and various N fertilizer rates and straw and water management practices (Figure 5). Site average seasonal CH<sub>4</sub> emissions across years ranged from 14 kg CH<sub>4</sub>-C ha<sup>-1</sup> to 477 kg CH<sub>4</sub>-C ha<sup>-1</sup>, while simulated averages ranged from 14 kg CH<sub>4</sub>-C ha<sup>-1</sup> to 646 kg CH<sub>4</sub>-C ha<sup>-1</sup>. Management-specific growing season emissions ranged from 10.9 kg CH<sub>4</sub>-C ha<sup>-1</sup> to 512 kg CH<sub>4</sub>-C ha<sup>-1</sup> across this validation data set, and on average, predictions of treatment means had an absolute relative deviation of 60.1% (Table 4). Within sites, the accuracy of modeled seasonal CH<sub>4</sub>

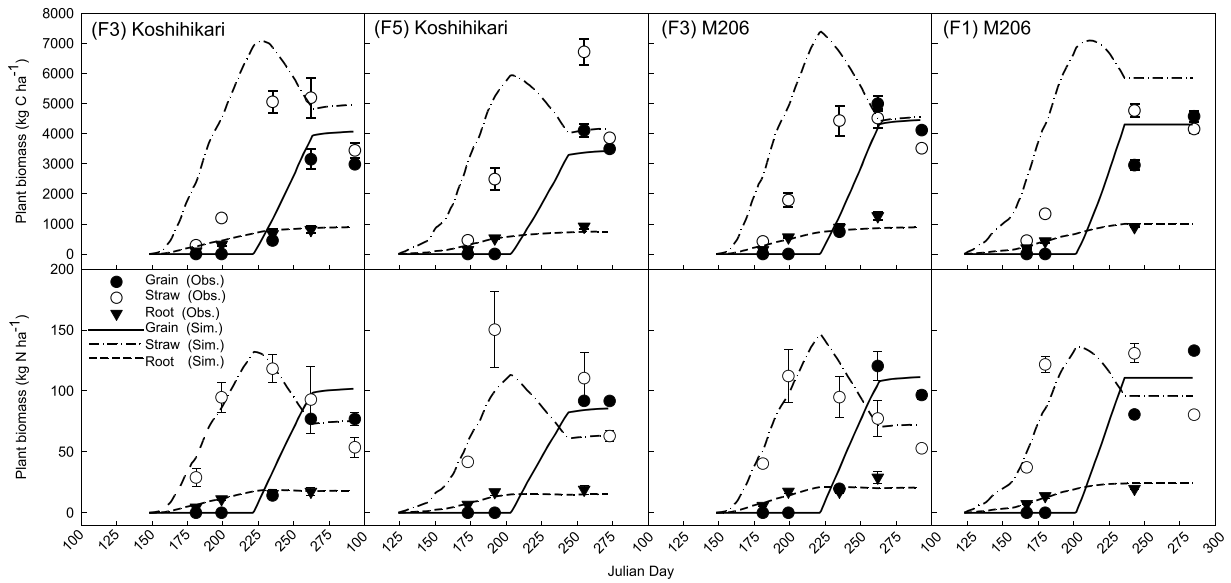


**Figure 3.** Calibrated and observed seasonal changes in plant (top row) C and (bottom row) N in grain, straw, and root biomass of Koshihikari and M206 during the 2011 growing season at F1, F3, and F5. Error bars represent the standard error of three replicates. Sampling dates coincided with (first to last) midtillering, panicle initiation, heading, field drainage, and maturity, except that there was no measurement at heading at F1 and F5. Note that these data are from the calibration data set.

emissions among the different management treatments varied (Figure 6 and Table 4). For example, in the side-by-side comparison of water-seeded, with stale seedbed or conventional tillage, and dry-seeded stale seedbed systems at F2, the model was unable to capture the magnitude of the mitigation effect of the dry-seeded system compared to the water-seeded systems (49–50% lower seasonal CH<sub>4</sub> emissions observed). However, there

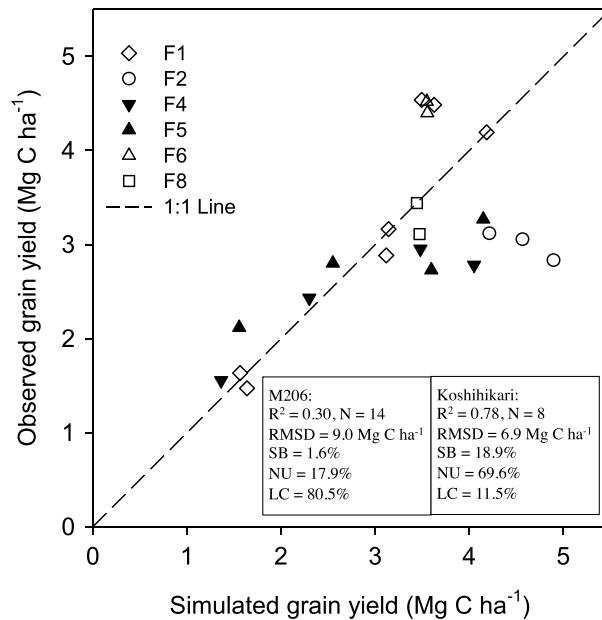


**Figure 4.** Model validation of grain C yield at six sites (F1, F2, F4, F5, F6, and F8). M206 and Koshihikari cultivars are represented by the white and black symbols, respectively. Note that study sites that grew M202 (F6 and F8) were simulated using a modified M206 calibration (see Table 3) and are represented by the M206 symbol. Root-mean-square deviation (RMSD) equates to deviations about the 1:1 line of equality, which is divided into three components: the squared bias (SB), nonunity slope (NU), and lack of correlation (LC).

was no apparent bias in overestimating or underestimating CH<sub>4</sub> emissions at sites that were all water seeded (F1, F6, and F7) or dry seeded (F4 and F5). Across all sites with N fertilizer treatments (F1, F2, and F5), the simulated response to N rate was greater than what was observed; the model simulated a large increase in CH<sub>4</sub> emissions from soils without N fertilizer to those with N fertilizer added (i.e., from 0 kg N ha<sup>-1</sup> to either 80 or 100 kg N ha<sup>-1</sup>). However, similar to observations, the modeled N fertilizer effect was not linear; above a certain midrange N rate, simulated CH<sub>4</sub> emissions declined and/or were stabilized at the highest N rates of 200 or 260 kg N ha<sup>-1</sup>. Across all sites with varying fallow period straw and water management practices (F6–F8), modeled seasonal CH<sub>4</sub> emissions were similar (i.e., not sensitive to different practices) following both straw burning and straw incorporation and winter flooding and no winter flooding, which agreed with two of the four site-year combinations (F8 and the first year at F7) where no statistically significant differences

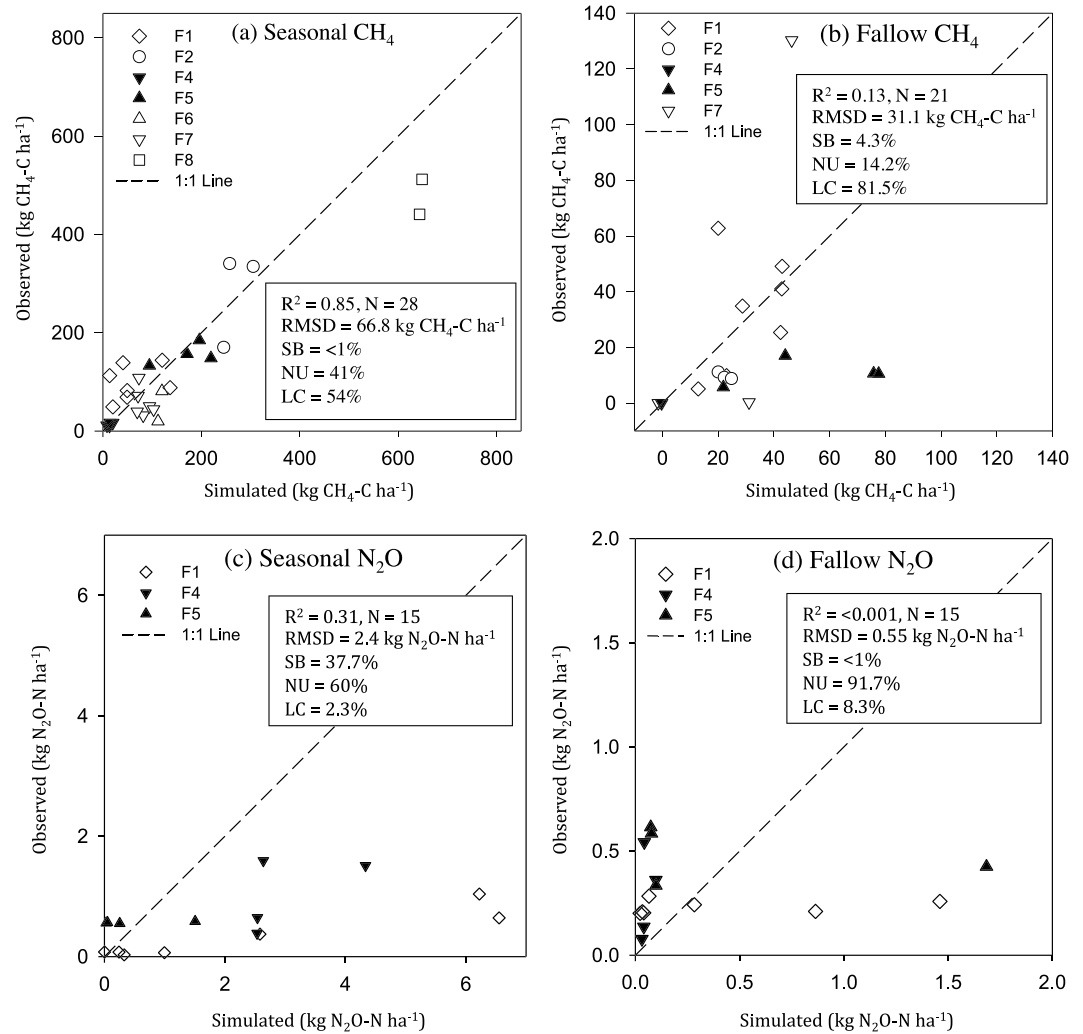


**Figure 5.** Model validation of cumulative CH<sub>4</sub> emissions during the (a) growing season and (b) fallow period and cumulative N<sub>2</sub>O emissions during the (c) growing season and (d) fallow period. Root-mean-square deviation (RMSD) equates to deviations about the 1:1 line of equality, which is partitioned into three components: the squared bias (SB), nonunity slope (NU), and lack of correlation (LC). M206 and Koshihikari cultivars are represented by the white and black symbols, respectively. Note that the sites that grew M202 (Table 2) were simulated using a modified M206 calibration (Table 3) and are represented by the M206 symbol.

were observed. However, the model was unable to capture the higher seasonal CH<sub>4</sub> emissions observed when no winter flooding preceded the growing season (second year at F7) or the lower seasonal CH<sub>4</sub> emissions observed when straw was burned compared to incorporated (F6 and second year at F7) (Figure 6 and Table 4).

The general temporal pattern of observed CH<sub>4</sub> efflux during the growing season was characterized by an increase in CH<sub>4</sub> emissions of variable duration, followed by a decline starting sometime between panicle initiation and flowering (Figure 6). The CH<sub>4</sub> efflux started sometime within 2 months after the initial permanent flood. Spikes in CH<sub>4</sub> emissions were observed following field drainage at the end of the growing season. Agreement between modeled and observed seasonal patterns was highly variable across sites and treatments. For example, the simulation of the initial increase in CH<sub>4</sub> emissions at F2 was closer to the observed fluxes in the dry-seeded treatment (51% average absolute relative deviation) than for the two water-seeded treatments, for which the increase in CH<sub>4</sub> emissions was underestimated by 95% on average due to a delay in the increase. At F8 seasonal CH<sub>4</sub> patterns were poorly simulated for both straw-incorporated and straw-burned treatments due to a delay and overestimation of the extent of the

**Table 4.** Comparison Between Simulated and Observed Mean Seasonal CH<sub>4</sub> Emissions

Study Site	Year	Treatment (Table 2)	CH <sub>4</sub> Emissions			Relative Deviation With Respect to Observed
			Observed	SE <sup>a</sup>	Simulated	
			(kg CH <sub>4</sub> -C ha <sup>-1</sup> Season <sup>-1</sup> )			
F1 (N = 7) <sup>b</sup>	2010	0N	49.1	26.1	20.2	-58.9%
		80N	88.2	17.1	136.5	54.8%
		140N <sup>c</sup>	79.5	9.8	68.1	
		200N	82.4	20.5	49.4	40.1%
		260N	68.9	7.3	49.3	28.5%
	2011	0N	112.9	2.3	13.6	-87.9%
		80N	144.0	16.6	120.7	-16.2%
		140N <sup>c</sup>	161.2	18.2	60.2	
		200N <sup>c</sup>	156.5	8.7	40.9	
		260N	139.0	10.9	40.8	-70.6%
F2 (N = 3)	2008	WSCON	334.7	18.7	309.5	-8.7%
		WSSSB	340.5	57.6	258.6	-24.3%
		DSSSB	170.2	32.3	245.6	44.3%
F3	2011	M206 cultivar <sup>c</sup>	74.2	7.7	67.4	
		KOSH cultivar <sup>c</sup>	83.3	27.5	51.1	
F4 (N = 4)	2010	0N	11.2	4.7	8.4	-25.3%
		50N	10.9	0.9	13.4	23.4%
		100N <sup>c</sup>	9.2	2.6	26.8	
		150N	16.7	5.0	20.0	20.0%
		200N	17.0	4.2	14.9	-12.5%
F5 (N = 4)	2011	0N	133.2	30.8	94.6	-29.0%
		50N	148.3	12.5	219.6	48.1%
		100N <sup>c</sup>	154.8	32.4	230.3	
		150N	185.0	39.4	196.2	6.1%
		200N	157.1	26.1	171.1	8.9%
F6 (N = 2)	1997	FF and SI	81.3	NA	120.2	47.7%
		FF and SB	19.8	NA	112.0	464.8%
F7 (N = 6)	1995	FF and SI	50.5	NA	94.8	87.6%
		FF and SB	31.8	NA	82.0	126.8%
		NFF and SI	44.1	NA	103.1	133.9%
	1996	FF and SI	71.6	NA	71.5	-0.2%
		FF and SB	39.4	NA	69.6	77.2%
		NFF and SI	108.3	NA	73.3	-32.3%
F8 (N = 2)	1992	FF and SI	512.1	NA	648.9	26.7%
		FF and SB	441.0	NA	643.8	46.0%

<sup>a</sup>Standard error of observed values.

<sup>b</sup>Sample size per study site used for validation.

<sup>c</sup>Calibration only.

increase in CH<sub>4</sub> emissions. Similarly, there was a delay in simulated CH<sub>4</sub> emissions for all N rate treatments the second year at F1, resulting in delayed peak emissions during the flooded period.

Fallow period CH<sub>4</sub> emissions remained relatively low across all treatments and sites, with the exception of the straw-incorporated treatment at F7 (Figure 6). In general, the temporal patterns of CH<sub>4</sub> emission observations during the fallow period were poorly simulated, particularly for cases with winter flood management. Two major discrepancies in the simulations were the rapid increase in CH<sub>4</sub> fluxes during the first couple of months of the winter flood, which was not observed at any of the sites (F1, F4, F5, and F7), and the missed spikes in CH<sub>4</sub> emissions following field drainage in the spring. Additionally, in one case, fallow period CH<sub>4</sub> emissions were greatly underestimated for the last couple of months of the fallow season flood for the treatment with straw incorporated.

The sensitivity to soil bulk density, root biomass ratio, and N<sub>2</sub> fixation parameters was tested at the F2 study site for the three seeding systems (Tables 5–7). As bulk density increased from 0.51 to 1.53 g cm<sup>-3</sup> (±50% of the measured value of 1.02 g cm<sup>-3</sup>), seasonal CH<sub>4</sub> emissions decreased (Table 5). While the sensitivity in soil bulk density in the water-seeded conventional system ranged from +17% to -15% the baseline value, the

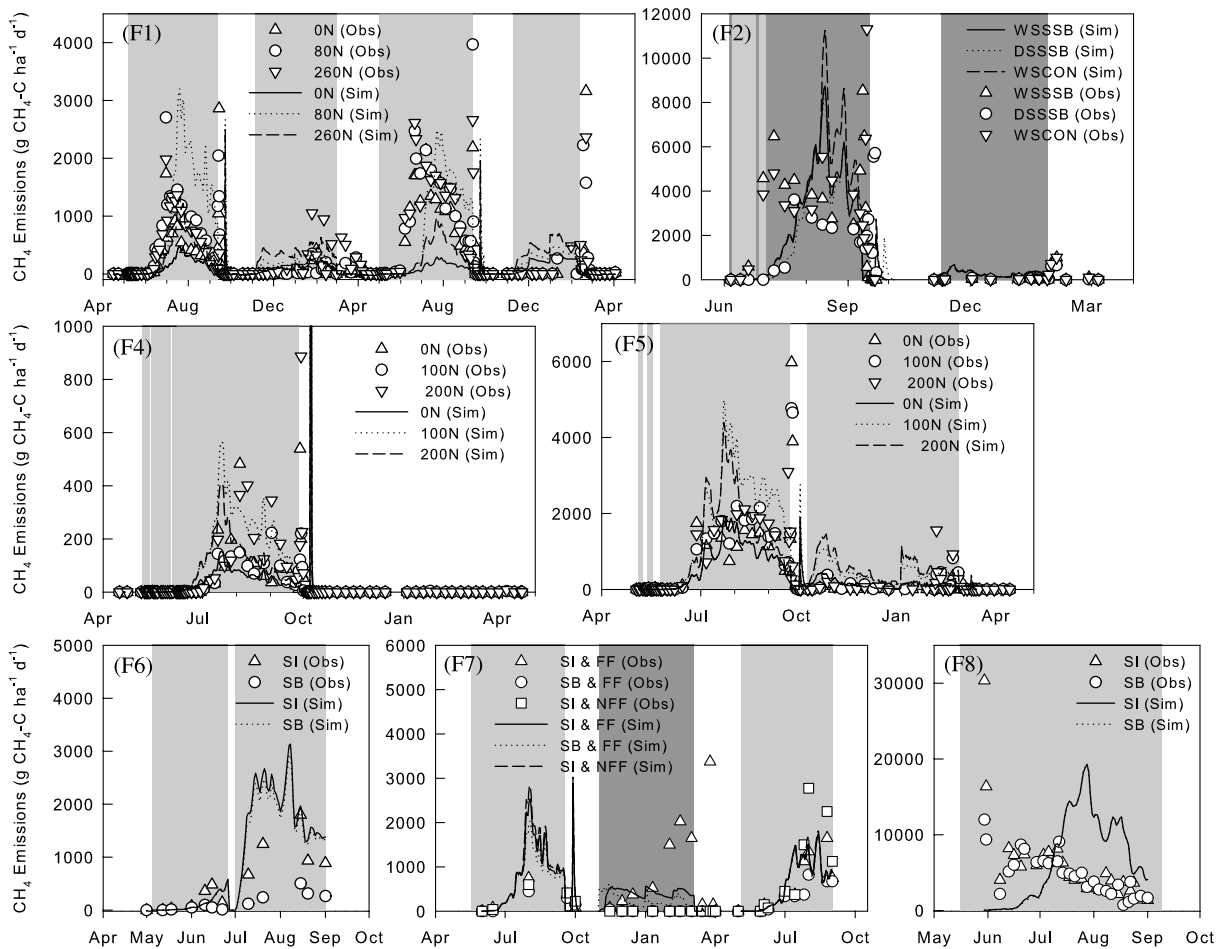


**Figure 6.** Comparison between observed (obs) and simulated (sim) daily fluxes of CH<sub>4</sub> emissions from rice fields under various management treatments (see Table 2) at F1, F2, and F4–F8. Flooded periods for all treatments are represented by the light grey shaded areas for all sites except F2 and F7; at F7 light grey represents flooding for all treatments, while dark grey represents fallow period flood treatments (FF), and at F2 the dark grey shaded areas represent flooding for the drill-seeded stale seedbed treatment (DSSSB), while both the dark grey and light grey represent flooding for the water-seeded treatments (WSCON and WSSSB). Note that both 100N treatments (100 kg N ha<sup>-1</sup>) at F4 and F5 were used for calibration only.

effect in the two stale seedbed systems was minimal (+3.1% to –1.2%). There was a positive correlation between the ratio of root C to total plant C and seasonal CH<sub>4</sub> emissions. Changes of ±50% of the root C ratio (0.09 for M206) resulted in large changes in seasonal CH<sub>4</sub> emissions across all three seeding systems (–61% to +183% on average) (Table 6). The relationship between the N<sub>2</sub> fixation index and seasonal CH<sub>4</sub> emissions

**Table 5.** Sensitivity of Modeled Seasonal CH<sub>4</sub> Emissions to Changes in Soil Bulk Density for the Three Seeding System Treatments at F2 (Table 1)<sup>a</sup>

Seeding System	Change in Bulk Density (%)								
	–50	–25	–15	–10	0	+10	+15	+25	+50
	<i>kg CH<sub>4</sub>-C ha<sup>-1</sup> Season<sup>-1</sup></i>								
Water-seeded conventional	358	331	325	322	306	297	295	275	261
Water-seeded stale seedbed	259	259	258	258	258	257	257	257	255
Dry-seeded stale seedbed	253	248	247	246	246	245	244	243	243
	<i>Change (%)</i>								
Water-seeded conventional	17.1	8.2	6.2	5.3	0	–3	–4	–10	–15
Water-seeded stale seedbed	0.3	0.3	0.1	0.1	0	–0.4	–0.4	–0.4	–1.0
Dry-seeded stale seedbed	3.1	1.0	0.6	0.4	0	–0.3	–0.6	–1.2	–1.2

<sup>a</sup>The baseline (0% change) bulk density value was 1.02 g cm<sup>-3</sup>.

**Table 6.** Sensitivity of Modeled Seasonal CH<sub>4</sub> Emissions to Changes in Root Biomass Ratio for the Three Seeding System Treatments at F2 (Table 1)<sup>a</sup>

Seeding System	Change in Root Biomass Ratio (%)				
	-50	-25	0	+25	+50
	<i>kg CH<sub>4</sub>-C ha<sup>-1</sup> Season<sup>-1</sup></i>				
Water-seeded conventional	113	161	306	572	921
Water-seeded stale seedbed	112	150	258	450	718
Dry-seeded stale seedbed	91	132	246	437	666
	<i>Change (%)</i>				
Water-seeded conventional	-63	-47	0	87	201
Water-seeded stale seedbed	-57	-42	0	74	178
Dry-seeded stale seedbed	-63	-46	0	78	171

<sup>a</sup>The baseline (0% change) root biomass ratio value was 0.09.

was less straightforward and depended on the seeding system. Similar to the other two parameters, model sensitivity was greatest in the water-seeded conventional system; with a -10% change in the N<sub>2</sub> fixation index (i.e., 6% plant N from N fixation), seasonal CH<sub>4</sub> emissions increased by 164% (Table 7). Across all seeding systems, there was a decline (-4.2 to -20%) in seasonal CH<sub>4</sub> emissions with a 10% increase in the N fixation index (i.e., 30% plant N from N<sub>2</sub> fixation). However, at higher N<sub>2</sub> fixation levels there was minimal additional effect on CH<sub>4</sub> emissions across all seeding systems.

### 3.3. Nitrous Oxide Emissions

Observed cumulative N<sub>2</sub>O emissions were minimal during the rice growing season and winter fallow period, ranging from 0.03 to 1.6 kg N<sub>2</sub>O-N ha<sup>-1</sup> and from 0.1 to 0.6 kg N<sub>2</sub>O-N ha<sup>-1</sup>, respectively, across three study sites (N = 15) to which a gradient of N fertilizer rate treatments were applied (Figure 5 and Table 8). The model explained 31% of the observed variation in cumulative growing season N<sub>2</sub>O emissions (RMSD = 2.4 kg N<sub>2</sub>O-N ha<sup>-1</sup>) but failed to simulate cumulative fallow period emissions (R<sup>2</sup> < 0.001, RMSD = 0.6 kg N<sub>2</sub>O-N ha<sup>-1</sup>) (Figure 5). On average, the model was most accurate at simulating growing season N<sub>2</sub>O emissions in F5 and least accurate in F1, with 99.3% and 685.2% average absolute relative deviation across the treatments, respectively (Table 8). Daily and cumulative N<sub>2</sub>O emissions were overestimated in most cases, particularly at higher N fertilizer rates (Figure 7). The timing of some peaks following field drainage events (Figure 7) and during precipitation events (precipitation data not shown) were captured fairly well. However, most fluxes were either missed by the model or occurred when no fluxes were observed, particularly when fields were initially flooded at the water-seeded site (F1) and during the early-season flush irrigation events at the dry-seeded sites (F4 and F5).

Discrepancies between simulated and observed seasonal N<sub>2</sub>O emissions were highly variable across all N fertilizer treatments, including the 0N controls, with a range of 54% to 1425% absolute relative deviations (Table 8). The model captured the observed stimulatory effect of N fertilizer additions on growing season

**Table 7.** Sensitivity of Modeled Seasonal CH<sub>4</sub> Emissions to Changes in N Fixation Index (Crop N/From Soil N) for the Three Seeding System Treatments at F2 (Table 1)<sup>a</sup>

Seeding System	Change in N Fixation Index (%)					
	-10	0	+10	+15	+25	+50
	<i>kg CH<sub>4</sub>-C ha<sup>-1</sup> Season<sup>-1</sup></i>					
Water-seeded conventional	806	306	244	228	225	235
Water-seeded stale seedbed	382	258	246	238	226	237
Dry-seeded stale seedbed	227	246	235	227	224	223
	<i>Change (%)</i>					
Water-seeded conventional	164	0	-20	-26	-26	-23
Water-seeded stale seedbed	48	0	-5	-8	-12	-8.2
Dry-seeded stale seedbed	-7	0	-4.2	-7.6	-8.6	-9.1

<sup>a</sup>The baseline (0% change) N fixation index was 1.18.

**Table 8.** Comparison Between Simulated and Observed Mean Seasonal N<sub>2</sub>O Emissions

Study Site	Year	Treatment (Table 2)	N <sub>2</sub> O Emissions			Relative Deviation With Respect to Observed
			Observed	SE <sup>a</sup>	Simulated	
			(kg N <sub>2</sub> O-N ha <sup>-1</sup> Season <sup>-1</sup> )			
F1 (N = 7) <sup>b</sup>	2010	0N	0.03	0.01	0.33	1043.0%
		80N	0.07	0.01	1.00	1424.5%
		140N <sup>c</sup>	0.22	0.09	1.27	
		200N	0.37	0.06	2.58	591.1%
		260N	1.04	0.19	6.22	498.6%
	2011	0N	0.08	0.04	0.00	-96.6%
		80N	0.07	0.04	0.24	223.9%
		140N <sup>c</sup>	0.17	0.04	0.48	
		200N <sup>c</sup>	0.42	0.05	2.12	
		260N	0.64	0.04	6.55	918.5%
F3	2011	M206 cultivar <sup>c</sup>	0.02	0.02	2.76	
		KOSH cultivar <sup>c</sup>	0.01	0.01	2.85	
F4 (N = 4)	2010	0N	0.39	0.02	2.54	553.8%
		50N	0.65	0.07	2.54	293.0%
		100N <sup>c</sup>	0.69	0.20	2.55	
		150N	1.59	0.18	2.64	65.7%
		200N	1.51	0.45	4.33	186.9%
F5 (N = 4)	2011	0N	0.56	0.18	0.03	-94.3%
		50N	0.57	0.19	0.05	-91.1%
		100N <sup>c</sup>	0.55	0.19	0.09	
		150N	0.55	0.19	0.26	-53.6%
		200N	0.58	0.21	1.51	158.0%

<sup>a</sup>Standard error of observed values.  
<sup>b</sup>Sample size per study site used for validation.  
<sup>c</sup>Calibration only.

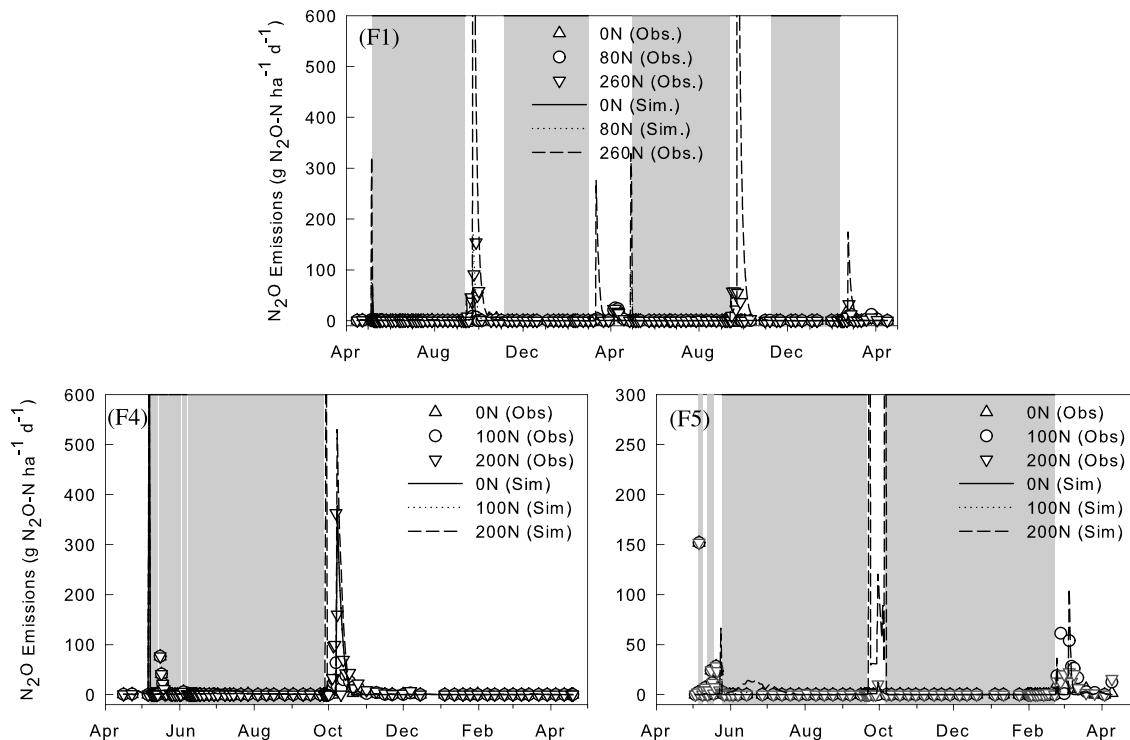


**Figure 7.** Comparison between observed (obs) and simulated (sim) daily fluxes of N<sub>2</sub>O emissions from rice fields under various management treatments (Table 2) at F1, F4, and F5 (Table 1). Flooded periods are represented by the shaded area. Note that both 100N treatments at F4 and F5 were used for calibration only.

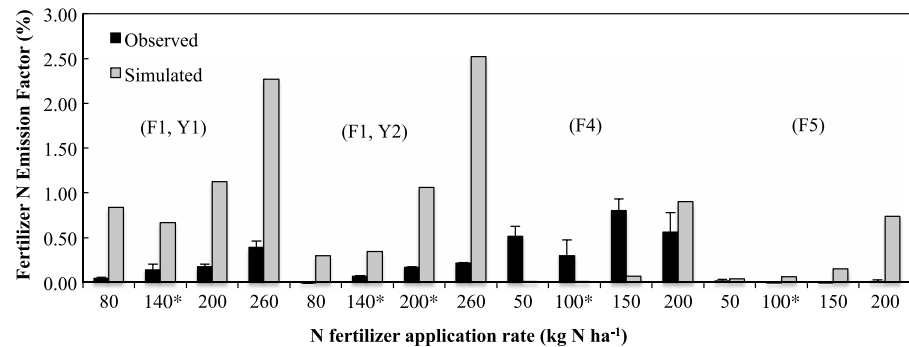


**Figure 8.** Observed and simulated fertilizer N-induced  $\text{N}_2\text{O}$  emission factors calculated for the growing season, across a gradient of fertilizer N additions at F1 in 2010 (Y1), F1 in 2011 (Y2), F4 in 2010, and F5 in 2011. Error bars represent the standard error of three replicates. Note that fertilizer N rates followed by an asterisk are from the calibration data set.

$\text{N}_2\text{O}$  emissions at F1 and F4. However, fertilizer N-induced  $\text{N}_2\text{O}$  emissions were also predicted at F5, but the effect was not observed there (Figure 8 and Table 8). Across sites, observed and simulated fertilizer N-induced  $\text{N}_2\text{O}$  emission factors ranged from 0% to 0.8% and from 0.01% to 2.5%, respectively (Figure 8). The model overestimated the N fertilizer contributions to seasonal  $\text{N}_2\text{O}$  emissions, especially at the highest N rates at all sites except F4. The model generally simulated increasing emission factors with increasing N rates across all sites, but this relationship was only observed at the water-seeded site F1, and not at either of the dry-seeded sites. Observed N fertilizer contributions to seasonal  $\text{N}_2\text{O}$  emissions were negligible at F5 regardless of the rate of fertilizer application (fertilizer N-induced  $\text{N}_2\text{O}$  emission factors less than 0.02%).

#### 4. Discussion

We tested the process-based model, DNDC, against measured growing season and fallow period emissions of  $\text{CH}_4$  from seven rice fields (three of which also had  $\text{N}_2\text{O}$  data) representing a wide range of soil types, weather patterns (seven distinct years between 1992 and 2012), and varying management practices in the primary rice-growing region in California, USA. This is the first study to evaluate the model performance of DNDC in simulating  $\text{CH}_4$  and  $\text{N}_2\text{O}$  emissions within direct-seeded rice systems, during the growing season and fallow period, and in a Mediterranean climate.

##### 4.1. Seasonal $\text{CH}_4$ Emissions

Eighty-five percent of variation in seasonal  $\text{CH}_4$  emissions was predicted across soil types at both water-seeded and dry-seeded sites (Figure 6) yet with some exceptions and discrepancies for particular management treatments within each site (e.g., straw burned and dry seeded). Half of all the simulations of seasonal  $\text{CH}_4$  emissions across sites had absolute relative deviations  $< 32\%$  ( $N=28$ ), and all nine site-years had at least one treatment with an absolute relative deviation  $< 29\%$ , with only two exceptions (F6 and the first year at F7) (Table 4).

Similarly, *Cai et al.* [2003] found all DNDC simulations of seasonal  $\text{CH}_4$  emissions from eight field sites across China to have  $< 33\%$  absolute relative deviation ( $N=17$ ), whereas across four sites in Thailand ( $N=6$ ) there was only one case with absolute relative deviation  $< 33\%$ . However, the flux data tested by *Cai et al.* [2003] were not all comparisons of treatments within the same sites; only four direct comparisons were made between treatments within the same site and year in China. Thus, there was potential for overfitting the model to a particular treatment or management routine within a site. In the present study, observed data showed that the response of seasonal  $\text{CH}_4$  emissions to the different management treatments (N fertilizer application rate or fallow period straw and water management) were highly variable across sites, which may be attributed to site by management treatment interactions, as well as in-field spatial heterogeneity of soil properties, such as soil organic C, pH, and temperature [Simmonds et al., 2013]. We also found that model sensitivity to one-at-a-time changes to three input parameters (i.e., soil bulk density, root C biomass to total plant C ratio, and  $\text{N}_2$  fixation index) at the F2 site, under the three distinct seeding systems, depended on the type of seeding system. This suggests an interaction between the management practice and the crop and soil input parameters.

#### 4.1.1. Effect of N Fertilizer Rate on Growing Season Emissions

The model predicted a wider range in seasonal CH<sub>4</sub> emissions than observed within all three of the sites with N fertilizer rate treatments (F1, F4, and F5), suggesting that the model is oversensitive to N fertilizer rates. However, this did not necessarily lead to large discrepancies in overall cumulative emissions at these sites, as was the case at F4 which had the lowest absolute relative deviation between site average of observed treatments and site average of modeled treatments (1.6%). Rather, the level of model sensitivity was inconsistent across the sites, showing an interaction among the site-specific ecological factors: weather, soil properties, and management routines, including the N fertilizer rate. *Cai et al.* [2003] found that the sensitivity of DNDC to various soil properties and management practices (e.g., fraction of litter returned to soil) depended on the site. In the present study, F1, F4, and F5 represent sites with different weather due to varying years and/or different weather stations from which data were measured. There is also a difference in soil texture among the sites; F1 and F4 were clay-textured soils, whereas F5 was a loam-textured soil (Table 1). Studies have reported a high sensitivity of DNDC to clay content [e.g., *Babu et al.*, 2006; *Li et al.*, 2004]. Clay content has an inhibitory effect on CH<sub>4</sub> emissions by reducing ebullition through greater entrapment of CH<sub>4</sub> [*Wang et al.*, 1993] and through physical protection of SOC from decomposition [*Baldock and Skjemstad*, 2000]. The negative effect of clay content on CH<sub>4</sub> emissions is expressed in DNDC through the inhibition of CH<sub>4</sub> diffusion across the simulated soil layers (equation (11)). The overestimated response to N rate at F5 may have been due to a greater interaction between clay mineral surfaces and SOC than could be predicted by clay content alone. However, the discrepancies were generally low at this site (i.e., < 29% for three of the four validation points). At F1, where there were only two input rates in the validation data set in the second year, 80 and 260 kg N ha<sup>-1</sup>, the emissions had a comparably low relative discrepancy.

There is high uncertainty in the net effect of N fertilizer additions, particularly ammonium-based fertilizers, on CH<sub>4</sub> emissions at any site given N rate alone, due to competing effects of N fertilizer addition on the production, oxidation, and transport of CH<sub>4</sub> at different levels of organization (i.e., plant or ecosystem level, microbial-community level, or biochemical level) [*Schimel*, 2000; *Cai et al.*, 2007]. This may be due to differences in plant growth response to N fertilizer across sites due to varying environmental conditions and management practices [e.g., *Linquist et al.*, 2009; *Peng and Cassman*, 1998; *Peng et al.*, 2010]. The primary sources of C for methanogens, DOC and CO<sub>2</sub>, are primarily derived from the rice roots via root exudation and turnover (rhizodeposition) [*Lu et al.*, 2000b] and root respiration [*Xu et al.*, 2008], respectively (equations (2) and (5)). Thus, if the growth response of rice to N fertilizer is greater in a poor soil compared to a fertile soil, the response of CH<sub>4</sub> emissions to N fertilizer additions may also be greater in a poor soil. Indeed, simulated seasonal CH<sub>4</sub> emissions were highly sensitive to changes in the root to total biomass ratio (Table 6). Root biomass inherently drives CH<sub>4</sub> production [*Aulakh et al.*, 2001a, 2001b], making accurate crop growth simulations crucial for CH<sub>4</sub> simulations.

Process-based models can only be as accurate as our understanding of the system, which is still progressing. There are contradictory reports of the net effect of N fertilization on CH<sub>4</sub> efflux from rice fields [*Cai et al.*, 2007]; some studies report an inhibitory effect [e.g., *Xie et al.*, 2010; *Yao et al.*, 2012], no effect [*Adviento-Borbe et al.*, 2013; *Pittelkow et al.*, 2014a; *Wang et al.*, 2012], or a stimulatory effect at low N rates and inhibitory effect at high N rates [*Linquist et al.*, 2012a]. Similar to *Banger et al.* [2012], who found a positive response of CH<sub>4</sub> emissions to N fertilization, especially at N rates less than 140 kg N ha<sup>-1</sup>, the greatest stimulatory effect was simulated at the lower end of the N rate treatments (i.e., < 150 kg N ha<sup>-1</sup> at F4, < 100 kg N ha<sup>-1</sup> at F5, and ≤ 140 kg N ha<sup>-1</sup> at F1) (Table 4). However, there were no significant differences reported among the N fertilizer rate treatments at either of the dry-seeded sites (F4 and F5), or the first year at the water-seeded site (F1), but at the second year a significant N fertilizer effect was reported (i.e., 0 kg N ha<sup>-1</sup> treatment < 80, 140, and 200 kg N ha<sup>-1</sup> treatments). Additionally, the model predicted an inhibitory effect at higher N rates, which was also reported in *Linquist et al.* [2012a] based on a meta-analysis of 24 field studies. However, the negative effect on CH<sub>4</sub> emissions at high N rates was not reported statistically significant at any of the sites in the current study. The discrepancy could partly be due to insufficient representation of the complex mechanisms at the various levels of organization [*Schimel*, 2000], as well as uncertainty in internal model parameters and the spatiotemporal variation in environmental drivers of C and N dynamics within each field. The model predicts an average net effect of the input data, using the same mean soil data for each treatment when, in fact, there can be high spatial variability within rice fields [*Simmonds et al.*, 2013]. This can result in particularly high prediction errors when responses to various drivers of CH<sub>4</sub> emissions are nonlinear.

#### 4.1.2. Effects of Fallow Period Straw and Water Management on Growing Season Emissions

The importance of fallow period management of straw and water on CH<sub>4</sub> emissions during the following growing season has been demonstrated in rice systems [Fitzgerald *et al.*, 2000; Yan *et al.*, 2005]. The Tier 1 method used to estimate seasonal CH<sub>4</sub> emissions in the IPCC Guidelines for National Greenhouse Gas Inventories for rice cultivation uses scaling factors, derived from field data, that account for the timing of straw incorporation and flooding prior to the growing season [Lasco *et al.*, 2006]. Rice soils typically have higher seasonal CH<sub>4</sub> emissions when flooded during the previous fallow period compared to drained conditions [Shiratori *et al.*, 2007; Yan *et al.*, 2005; Xu and Hosen, 2010]. This stimulatory effect from flooding during the fallow period has been attributed to lower soil Eh at the start of the growing season, effectively priming methanogenesis as it requires thoroughly reduced conditions to occur [Xu and Hosen, 2010]. The timing of rice straw incorporation also affects growing season CH<sub>4</sub> emissions. When straw is incorporated at the end of the fallow period, immediately prior to rice cultivation, rather than the beginning of the fallow period, higher seasonal CH<sub>4</sub> emissions are typical [Lu *et al.*, 2000a; Watanabe and Kimura, 1998; Xu *et al.*, 2000]. Additionally, higher application rates of rice straw during the fallow period lead to higher CH<sub>4</sub> emissions in subsequent growing seasons [Lu *et al.*, 2000a; Watanabe and Kimura, 1998; Xu and Hosen *et al.*, 2010].

The carryover effect of some of these fallow period management practices was tested at three of the sites (F6–F8) with a total of four site-year combinations. Although the greatest absolute relative deviation between simulated and mean observed seasonal CH<sub>4</sub> emissions across all treatments and sites ( $N = 28$ ) was the straw burned (SB) treatment at F6 (465%), the greatest discrepancies for all treatments at a particular study site occurred the first year at F7 (Table 4). The discrepancies at F7 may in part be due to measurement error due to a very limited number of observations during the first year of the study, particularly during the period with highest emissions, as opposed to inaccuracy of the model (Figure 6). However, the model was limited in its capacity to accurately simulate the inhibitory effect of straw burning on seasonal CH<sub>4</sub> emissions across all sites with CH<sub>4</sub> emissions overestimated > 45% (Table 4). A potential reason for this overestimation is that the burned straw residue (i.e., black C) remaining after burning can be more recalcitrant than unburned straw [Lehmann *et al.*, 2006], yet the model can only be adjusted for burned straw management by reducing the proportion of straw residue left in the field after harvest (ranged from 7% to 45%, in comparison to 100% for the straw incorporated treatments). The primary postharvest straw management practice in California is soil incorporation due to state regulations in 1991 that reduced rice straw burning due to air pollution [Hill *et al.*, 2006]. Since up to 25% of rice straw is still burned in California [Hill *et al.*, 2006], it will be important to improve the scientific structure of this aspect of the model for application at the regional scale.

Contrary to other studies [Xu *et al.*, 2003; Yan *et al.*, 2005; Xu and Hosen, 2010], at F7 seasonal CH<sub>4</sub> emissions were 51.2% greater without prior fallow period flooding and straw incorporation (NFF and SI) than with fallow period flooding and straw incorporation (FF and SI) (Table 4). However, there was minimal differentiation in simulated seasonal CH<sub>4</sub> emissions among all of the treatments at F7 and a large underestimation in fallow period CH<sub>4</sub> emissions in the FF and SI. Based on the higher fallow period CH<sub>4</sub> efflux that was observed in the FF and SI compared to the NFF and SI at F7 (Figure 6), the lower seasonal CH<sub>4</sub> emissions in FF and SI are presumably due to depletion of the C substrate pool due to high CH<sub>4</sub> production during the previous winter. Importantly, despite lower seasonal CH<sub>4</sub> emissions, annual CH<sub>4</sub> emissions in the FF and SI were greater compared to NFF and SI due to the high winter emissions in FF and SI. Due to the poor agreement between observed and simulated fallow period CH<sub>4</sub> emissions across all sites, the cause of the discrepancy of the underestimation of the model to prior fallow period water management is unclear. The discrepancy at F7 may be related to the cause of the underestimation in seasonal CH<sub>4</sub> emissions at F1 during the second year of the study, as F1 also had different fallow period water management practices preceding each growing season; there was no fallow period flood preceding the first growing season, but there was the second year, which had considerably higher seasonal emissions. Pittelkow *et al.* [2013] suggested that the stimulatory effect of winter flooding on seasonal CH<sub>4</sub> emissions may have caused the difference in annual emissions between both years. During the fallow period and beginning of the growing season, anaerobic decomposition and soil Eh dynamics in the simulated soil profile drive total substrate concentrations, their proportional allocation to inside or outside of the anaerobic balloon, and the rates of CH<sub>4</sub> production and oxidation (equations (3), (4), and (7)–(9)). Thus, there are clearly aspects of the decomposition and fermentation submodels that will need improvement to more

accurately describe winter fallow period C and N dynamics, as well as soil Eh dynamics during the transition from fallow period flooding (or no flooding) to the growing season. Additionally, the physical mechanisms of gas diffusion and ebullition in flooded rice fields without vegetation will also likely need to be improved upon based on the discrepancies in fallow period patterns of CH<sub>4</sub> emissions (equations (10)–(12)).

#### 4.1.3. Seeding System

Although the water-seeded method of rice establishment is the most common in California, dry-seeded systems have become more prevalent [Hill *et al.*, 2006]. Adoption of dry-seeding methods may increase as these methods are considered a potential CH<sub>4</sub> mitigation option in current proposals for C offset programs in California rice agriculture (i.e., Rice Cultivation Project Protocol, version 1.1, 2013, available from the Climate Action Reserve, <http://www.climateactionreserve.org>). Dry-seeded systems are sown with nongermminated rice seed into field-dry soil, and intermittent flush irrigation is applied to aid in seed germination for approximately 1 month. Thus, compared to water-seeded systems, dry-seeded systems have shorter duration of anaerobic soil conditions, which may reduce cumulative CH<sub>4</sub> emissions. With different seeding systems compared within the same field (F2), the model underestimated the CH<sub>4</sub> mitigation potential of dry seeding, compared to both water-seeded conventional (WSSCON) and water-seeded stale seedbed (WSSSB) systems. This was due in large part to both an underestimation of early-season CH<sub>4</sub> emissions in the water-seeded systems and overestimation of late-season CH<sub>4</sub> emissions in the dry-seeded system. Thus, the problem was the discrepancy in temporal variation in CH<sub>4</sub> emissions and in magnitudes of efflux among all systems. However, despite discrepancies in seasonal patterns of CH<sub>4</sub> efflux for the WS systems at F2, cumulative seasonal CH<sub>4</sub> emissions were in good agreement with the model (8.7% and –24.3% relative deviation, respectively) (Table 4). Based on the observed differences in seasonal patterns of CH<sub>4</sub> emissions between water-seeded and dry-seeded systems, it appears that the timing and rate at which CH<sub>4</sub> efflux increases early on in each system was the major distinction between the systems (i.e., earlier and greater rate of increase in CH<sub>4</sub> emissions in WS), although the DS system also sustained lower CH<sub>4</sub> efflux later on in the season (Figure 6). The simulated delay in early-season CH<sub>4</sub> emissions in the water-seeded systems may be due to an overestimation of the concentrations of Mn<sup>4+</sup>, Fe<sup>3+</sup>, and sulfate, and subsequently, the Eh buffering capacity at this site [Yao *et al.*, 1999].

While the model was unable to simulate the magnitude of the differences in seasonal CH<sub>4</sub> emissions between seeding systems within a single site, the model showed good agreement (absolute relative deviations < 29%) with observed seasonal CH<sub>4</sub> emissions for at least one of the treatments at both water-seeded and dry-seeded sites, excluding F6 and the first year at F7. This suggests that the capacity of the model to simulate distinctions between dry seeding and water seeding depends on the site-specific soil, crop, and climate input parameters. In order for the model to be utilized for predicting the mitigation potential of converting a water-seeded system to dry seeding, further studies will be needed to test these systems in side-by-side field experiments, across soil types, and coupled with mechanistic modeling.

#### 4.2. Fallow Period CH<sub>4</sub> and N<sub>2</sub>O Emissions

In direct-seeded rice fields with standard fertilizer N application rates and fallow period flooding and straw incorporation, reports on the contribution of fallow period GHG emissions to annual emissions have ranged from 3% [Pittelkow *et al.*, 2014b] to 61% [Fitzgerald *et al.*, 2000] for CH<sub>4</sub> and from 57% [Pittelkow *et al.*, 2013] to 76% for N<sub>2</sub>O [Adviento-Borbe *et al.*, 2013]. When rice fields are flooded during the winter, simulated CH<sub>4</sub> emissions are primarily controlled by (1) substrate concentrations predicted by SOC decomposition (equations (3) and (4)), (2) allocation of substrates to either CH<sub>4</sub> production or CH<sub>4</sub> oxidation routines (equations (7)–(9)) according to the anaerobic balloon concept, and (3) transport of CH<sub>4</sub> from soil to the atmosphere via diffusion and ebullition (equations (10) and (12)). Overestimation of fallow period CH<sub>4</sub> emissions (Figures 5 and 6) may partly be due to underestimation of the inhibitory effect of clay content on CH<sub>4</sub> diffusion (equation (11)) as well as on rates of decomposition of SOC (equation (3)). Additionally, the inhibitory effects of lower winter temperatures on SOC decomposition (equation (3)) and on ebullition (equation (12)) may have been underestimated. Large fluxes of CH<sub>4</sub> and N<sub>2</sub>O emissions were observed after drainage while soils dried out (Figures 6 and 7), which has been attributed to the physical gasification of entrapped dissolved CH<sub>4</sub> and denitrification- and/or nitrification-induced N<sub>2</sub>O emissions [Adviento-Borbe *et al.*, 2015]. Following drainage, the proportion of simulated dissolved CH<sub>4</sub> that is released as CH<sub>4</sub> versus oxidized to CO<sub>2</sub> depends on changing dissolved CH<sub>4</sub> concentrations and gradients between soil layers as soil moisture declines (equations (9),

(10), and (12)). Thus, lack of site-specific knowledge of soil hydraulic properties likely account for a large portion of the uncertainty in postdrainage CH<sub>4</sub> fluxes. Similarly, postdrainage spikes in simulated N<sub>2</sub>O emissions also depend on soil hydrology, although in this case due to its effect on microbial activity; with decreasing soil moisture, soil Eh and concentrations of NH<sub>4</sub><sup>+</sup> and nitrogenous oxide substrates increase, thereby affecting rates of denitrification and nitrification ((R1) and equations (14)–(17) and (24)).

### 4.3. Seasonal N<sub>2</sub>O Emissions

Across both the dry-seeded sites (F4 and F5) and the water-seeded site (F1), growing season N<sub>2</sub>O emissions occurred at the beginning of the growing season during flush irrigation events (dry-seeded fields) and following field drainage at the end of the growing season, when soil conditions have been reported to be optimal for both denitrification and nitrification processes to occur [Gauch *et al.*, 2003; Knowles, 2005; Adviento-Borbe *et al.*, 2015]. Water-seeded systems are planted with pregerminated seed and thus are continuously flooded during the growing season. In contrast, dry-seeded systems are planted with nongerminated seed and often require intermittent flushes of irrigation at the beginning of the growing season for seed germination. In most cases, seasonal N<sub>2</sub>O emissions were overestimated, indicated by the majority (60%) of the MSD partitioned to nonunity slope (Figure 5). This may partly be attributed to uncertainty in simulated soil hydrology during the flush irrigation events, which ultimately drives soil Eh and concentrations of substrates available for nitrification or denitrification. Higher N<sub>2</sub>O emissions are expected when fertilizer N is applied in excess of plant N requirements, as soil mineral N is otherwise expected to be low at the end of the growing season due to plant N uptake [Linquist *et al.*, 2006]. Accordingly, seasonal N<sub>2</sub>O emissions were generally higher in the N-fertilized plots compared to the 0N control (Table 8). These results are consistent with a meta-analysis that showed that on average, N<sub>2</sub>O emissions increased with N additions by 216% across managed and unmanaged ecosystems [Liu and Greaver, 2009]. However, in the present study the fertilizer N effect was overestimated in the simulations, resulting in inflated N fertilizer-induced N<sub>2</sub>O emission factors, especially at higher N rates (Table 8 and Figure 9). Fertilizer N was applied immediately prior to continuously flooding both the dry seeded (F4 and F5) and the water seeded (F1) fields. Thus, differences among N treatments were not apparent until after the end-of-season drain (Figure 7). One possible explanation for the oversensitivity of simulated N<sub>2</sub>O emissions to N fertilizer rate may be due to overestimating rate at which soils dried out following drainage and consequently the rate of increasing concentrations of nitrogenous substrates and soil Eh. These processes largely control the proportion of N<sub>2</sub>O that is emitted to the atmosphere versus reduced to N<sub>2</sub>. Second, the rates of SOM mineralization may have also been overestimated, which would inflate nitrification-induced N<sub>2</sub>O production (equation (24)).

In previous studies, there have been mixed reports on modeling seasonal N<sub>2</sub>O emissions in rice systems using DNDC. Similar to our findings, Cai *et al.* [2003] were unsuccessful in simulating seasonal N<sub>2</sub>O emissions from rice systems in China. Li *et al.* [2005] suggested that the reason for poor simulation of N<sub>2</sub>O emissions in rice fields tested by Cai *et al.* [2003] was due to insufficient knowledge of management input data. However, even with more site-specific information, if the calibration procedures are not described in detail, the underlying causes of improvement in model performance are not always obvious. Babu *et al.* [2005] and Pathak *et al.* [2005] reported generally good agreement between observed and simulated seasonal N<sub>2</sub>O emissions from rice fields in India. Whereas Pathak *et al.* [2005] reported a –6.8% relative deviation between modeled and observed seasonal N<sub>2</sub>O emissions in a single rice field in India, Babu *et al.* [2005] reported relative deviations ranging from –247.8% to 28.6% across two rice fields under various fertility treatments. The lower relative prediction errors made by Pathak *et al.* [2005] may be due to overfitting of the model to the individual field site, as only one site and year with a single treatment was used for the validation. While Pathak *et al.* [2005] do not describe whether input parameters were adjusted in the calibration process to match flux measurements, Babu *et al.* [2005] report changing the microbial activity index to correspond to emissions of CH<sub>4</sub> and N<sub>2</sub>O at two different sites, and the final value was then held constant for the validation sites.

Based on these results, further mechanistic revision of the model is needed for simulating seasonal N<sub>2</sub>O emissions in rice systems. Nitrous oxide emissions occur under moderately low redox conditions yet at soil moisture levels sufficiently greater than what is favorable for complete denitrification (i.e., N<sub>2</sub>O is reduced to N<sub>2</sub>) [Ciarlo *et al.*, 2007]. Thus, controlled experiments designed to test the individual components of (a) the soil climate submodel that describe the physical processes controlling soil moisture and redox conditions during

field drainage and (b) the decomposition and nitrification submodels that describe the biochemical processes driving N substrate availability during these important N<sub>2</sub>O efflux events may reduce uncertainty in predictions of N<sub>2</sub>O emissions.

## 5. Conclusions

Evaluating the performance of DNDC in simulating CH<sub>4</sub> and N<sub>2</sub>O emissions in side-by-side field trials of various management treatments is a necessary first step in determining the applicability of the model for quantifying GHG mitigation potentials of alternative practices and for extrapolation to larger spatial scales. New parameterizations for two distinct cultivar types (M206 and Koshihikari) were performed based on field measurements with satisfactory estimates of grain yield (RMSD = 0.90 Mg C ha<sup>-1</sup> and 0.69 Mg C ha<sup>-1</sup>, respectively) and seasonal dynamics of plant C and N, except for an overestimation in early-season C allocation to straw. Sensitivity tests showed that CH<sub>4</sub> emissions are most sensitive to the ratio of root C to total plant C, which implies that a lack of cultivar-specific knowledge will have a large impact on prediction of CH<sub>4</sub> emission. This study demonstrated that growing season CH<sub>4</sub> emissions in direct-seeded rice systems are generally well simulated, judged by at least one management treatment from seven of the nine site-year combinations having < 29% absolute relative deviation. However, there were discrepancies in temporal patterns irrespective of good agreement in cumulative CH<sub>4</sub> emissions. Given the wide range in observed seasonal CH<sub>4</sub> emissions across sites, a major strength of DNDC was in estimating general site-level seasonal CH<sub>4</sub> emissions. However, a major limitation was in simulating finer resolution of differences in CH<sub>4</sub> emissions (or lack thereof) among side-by-side management treatments (N fertilizer application rate, type of seeding system, fallow period straw, and water management). Additionally, DNDC did not satisfactorily simulate fallow period CH<sub>4</sub> emissions or seasonal and fallow period N<sub>2</sub>O emissions across all sites with the exception of a few cases (i.e., one site had three N rate treatments with absolute relative deviations of fallow period CH<sub>4</sub> emissions < 18%). Uncertainty in these predictions was attributed to uncertainty in both the input parameters due to in-field spatiotemporal variability of soil properties and in the model structure (e.g., clay effects, and simulation routines for field drainage, and diffusion and ebullition of gasses). These uncertainties will need to be improved and accounted for if DNDC is to be used for C offset programs or for extrapolating to regional scales. Although the majority of global warming potential from CH<sub>4</sub> and N<sub>2</sub>O emissions in rice fields is due to CH<sub>4</sub> emissions, more accuracy is needed in the model for predicting N<sub>2</sub>O emissions particularly when most mitigation practices target changes in water management that may increase N<sub>2</sub>O emissions. In order to fully account for mitigation potentials of management practices at the regional scale, DNDC model-directed mechanistic field studies are warranted to further explain management interactions with other site-specific environmental drivers. Isotope tracer studies could be used to constrain the simulated pathways of CH<sub>4</sub> and N<sub>2</sub>O production, as well as the sources of substrates (plant derived versus soil derived) in DNDC. Measurements of soil moisture, Eh, and SOC mineralization rates following field drainage, could also be used to improve model descriptions of soil water dynamics during this time and subsequent changes in soil Eh and substrate concentrations.

### Acknowledgments

The research was funded in part by Mars, Inc., as well as the William G. and Kathleen Golden International Agriculture Fellowship, UCD and Humanities Graduate Research Award, and the Department of Plant Sciences at the University of California, Davis, through a graduate student research assistantship awarded to Maegen Simmonds. Changsheng Li's participation in the study was partially supported by the USDA NIFA FACCE project "GreenRice" (110271). We thank the authors of the field experiments used in the model evaluation, especially Cameron Pittelkow and Arlene Adviento-Borbe, for providing detailed supplemental data sets. We also greatly appreciate the statistical consultations provided by Neil Willits from the University of California, Davis, and Bill Salas from Applied GeoSolutions for the help with model troubleshooting, supplying summary data of publications, and facilitating collaborations between University of California, Davis, and the University of New Hampshire.

## References

- Adviento-Borbe, M. A., C. M. Pittelkow, M. Anders, C. van Kessel, J. E. Hill, A. M. McClung, J. Six, and B. A. Linquist (2013), Optimal fertilizer nitrogen rates and yield-scaled global warming potential in drill seeded rice, *J. Environ. Qual.*, *42*(6), 1623–1634, doi:10.2134/jeq2013.05.0167.
- Adviento-Borbe, M. A., G. N. Padilla, C. M. Pittelkow, M. Simmonds, C. van Kessel, and B. Linquist (2015), Methane and nitrous oxide emissions from flooded rice systems following the end-of-season drain, *J. Environ. Qual.*, *44*(4), 1071–1079, doi:10.2134/jeq2014.11.0497.
- Aulakh, M. S., R. Wassmann, C. Bueno, J. Kreuzwieser, and H. Rennenberg (2001a), Characterization of root exudates at different growth stages of ten rice (*Oryza sativa* L.) cultivars, *Plant Biol.*, *3*(2), 139–148, doi:10.1055/s-2001-12905.
- Aulakh, M. S., R. Wassmann, C. Bueno, and H. Rennenberg (2001b), Impact of root exudates of different cultivars and plant development stages of rice (*Oryza sativa* L.) on methane production in a paddy soil, *Plant Soil*, *230*(1), 77–86, doi:10.1023/A:1004817212321.
- Babu, Y. J., C. Li, S. Frolking, D. R. Nayak, and T. K. Adhya (2006), Field validation of DNDC model for methane and nitrous oxide emissions from rice-based production systems of India, *Nutr. Cycling Agroecosyst.*, *74*(2), 157–174, doi:10.1007/s10705-005-6111-5.
- Baldock, J. A., and J. O. Skjemstad (2000), Role of the soil matrix and minerals in protecting natural organic materials against biological attack, *Org. Geochem.*, *31*(7–8), 697–710, doi:10.1016/S0146-6380(00)00049-8.
- Banger, K., H. Tian, and C. Lu (2012), Do nitrogen fertilizers stimulate or inhibit methane emissions from rice fields?, *Global Change Biol.*, *18*(1), 3259–3267, doi:10.1111/j.1365-2486.2012.02762.x.
- Baruah, K. K., B. Gogoi, and P. Gogoi (2010), Plant physiological and soil characteristics associated with methane and nitrous oxide emission from rice paddy, *Physiol. Mol. Biol. Plants*, *16*(1), 79–91, doi:10.1007/s12298-010-0010-1.
- Bird, J. A. (2001), Soil organic matter dynamics under alternative rice straw management practices, PhD dissertation, ProQuest, UMI Dissertations 3007663, Univ. of Calif., Davis.

- Bossio, D. A., W. R. Horwath, R. G. Mutters, and C. van Kessel (1999), Methane pool and flux dynamics in a rice field following straw incorporation, *Soil Biol. Biochem.*, *31*(9), 1313–1322, doi:10.1016/S0038-0717(99)00050-4.
- Brown, L., S. C. Jarvis, and D. Heaton (2001), A farm-scale basis for predicting nitrous oxide emissions from dairy farms, *Nutr. Cycling Agroecosyst.*, *60*(1–3), 149–158, doi:10.1023/A:1012659801484.
- Cai, Z., T. Sawamoto, C. Li, G. Kang, J. Boonjawan, A. Mosier, R. Wassmann, and H. Tsuruta (2003) Field validation of the DNDC mode for greenhouse gas emissions in East Asian cropping systems. *Global Biogeochem. Cycles*, *17*(4), 1107, doi:10.1029/2003GB002046.
- Cai, Z., Y. Shan, and H. Xu (2007), Effects of nitrogen fertilization on CH<sub>4</sub> emissions from rice fields, *Soil Sci. Plant Nutr.*, *53*(4), 353–361, doi:10.1111/j.1747-0765.2007.00153.x.
- Ciais, P., et al. (2013), 2013: Carbon and other biogeochemical cycles, in *Climate Change 2013: The Physical Science Basis, Contribution of Working Group I to the Fifth Assessment Report of the Intergovernmental Panel on Climate Change*, edited by T. F. Stocker et al., pp. 465–570, Cambridge Univ. Press, Cambridge, U. K., and New York.
- Ciarlo, E., M. Conti, N. Bartoloni, and G. Rubio (2007), The effect of moisture on nitrous oxide emissions from soil and the N<sub>2</sub>O/(N<sub>2</sub>O + N<sub>2</sub>) ratio under laboratory conditions, *Biol. Fertil. Soils*, *43*(6), 675–681, doi:10.1007/s00374-006-0147-9.
- Conrad, R. (2005), Quantification of methanogenic pathways using stable carbon isotopic signatures: A review and a proposal, *Org. Geochem.*, *36*(5), 739–752, doi:10.1016/j.orggeochem.2004.09.006.
- Eller, G., and P. Frenzel (2001), Changes in activity and community structure of methane-oxidizing bacteria over the growth period of rice, *Appl. Environ. Microbiol.*, *67*(6), 2395–2403, doi:10.1128/AEM.67.6.2395-2403.2001.
- Fitzgerald, G. J., K. M. Scow, and J. E. Hill (2000), Fallow season straw and water management effects on methane emissions in California rice, *Global Biogeochem. Cycles*, *14*(3), 767–776, doi:10.1029/2000GB001259.
- Gauch, H. G., Jr., J. T. G. Hwang, and G. W. Fick (2003), Model evaluation by comparison of model-based predictions and measured values, *Agron. J.*, *95*(6), 1442–1446, doi:10.2134/agronj2003.1442.
- Hill, J. E., J. F. Williams, R. G. Mutters, and C. A. Greer (2006), The California rice cropping system: Agronomic and natural resource issues for long-term sustainability, *Paddy Water Environ.*, *4*(1), 13–19, doi:10.1007/s10333-005-0026-2.
- Holzappel-Pschorn, A., R. Conrad, and W. Seiler (1986), Effects of vegetation on the emission of methane from submerged paddy soil, *Plant Soil*, *92*(2), 223–233, doi:10.1007/BF02372636.
- Horie, T., M. Ohnishi, J. F. Angus, L. G. Lewin, T. Tsukaguchi, and T. Matano (1997), Physiological characteristics of high-yielding rice inferred from cross-location experiments, *Field Crops Res.*, *52*(1–2), 66–67, doi:10.1016/S0378-4290(96)03458-2.
- Hou, A. X., G. X. Chen, Z. P. Wang, O. Van Cleemput, and W. H. Patrick Jr. (2000), Methane and nitrous oxide emissions from a rice field in relation to soil redox and microbiological processes, *Soil Sci. Soc. Am. J.*, *64*(6), 2180–2186, doi:10.2136/sssaj2000.6462180x.
- Knowles, R. (2005), Denitrifiers associated with methanotrophs and their potential impact on the nitrogen cycle, *Ecol. Eng.*, *24*(5), 441–446, doi:10.1016/j.ecoleng.2005.01.001.
- Ladha, J. K., D. Dawe, T. S. Ventura, U. Singh, W. Ventura, and I. Watanabe (2000), Long-term effects of urea and green manure on rice yields and nitrogen balance, *Soil Sci. Soc. Am. J.*, *64*(6), 1993–2001, doi:10.2136/sssaj2000.6461993x.
- Lasco, R. D., et al. (2006), Cropland, in *2006 IPCC Guidelines for National Greenhouse Gas Inventories, Agriculture, Forestry and Other Land Use*, vol. 4, edited by S. Eggleston et al., pp. 5.1–5.66, Institute for Global Environmental Strategies, Hayama, Japan.
- Lauren, J. G., G. S. Pettygrove, and J. M. Duxbury (1994), Methane emissions associated with a green manure amendment to flooded rice in California, *Biogeochemistry*, *24*(2), 53–65, doi:10.1007/BF02390179.
- Lehmann, J., J. Gaunt, and M. Rondon (2006), Bio-char sequestration in terrestrial ecosystems—A review, *Mitig. Adapt. Strat. Global Change*, *11*(2), 403–427, doi:10.1007/s11027-005-9006-5.
- Li, C. (2007), Quantifying greenhouse gas emissions from soils: Scientific basis and modeling approach, *Soil Sci. Plant Nutr.*, *53*(4), 344–352, doi:10.1111/j.1747-0765.2007.00133.x.
- Li, C. S. (2000), Modeling trace gas emissions from agricultural ecosystems, *Nutr. Cycling Agroecosyst.*, *58*(1–3), 259–276, doi:10.1023/A:1009859006242.
- Li, C. S., J. Qiu, S. Frolking, X. Xiao, W. Salas, B. Moore III, S. Boles, Y. Huang, and R. Sass (2002) Reduced methane emissions from large-scale changes in water management of China's rice paddies during 1980–2000, *Geophys. Res. Lett.*, *29*(20), 1972, doi:10.1029/2002GL015370.
- Li, C. S., A. Mosier, R. Wassmann, Z. Cai, X. Zheng, Y. Huang, H. Tsuruta, J. Boonjawan, and R. Lantin (2004), Modeling greenhouse gas emissions from rice-based production systems: Sensitivity and upscaling, *Global Biogeochem. Cycles*, *18*, GB1043, doi:10.1029/2003GB002045.
- Li, C. S., S. Frolking, X. Xiao, B. Moore III, S. Boles, J. Qiu, Y. Huang, W. Salas, and R. Sass (2005), Modeling impacts of farming management alternatives on CO<sub>2</sub>, CH<sub>4</sub>, and N<sub>2</sub>O emissions: A case study for water management of rice agriculture of China, *Global Biogeochem. Cycles*, *19*, GB3010, doi:10.1029/2004GB002341.
- Li, C., S. Frolking, and T. A. Frolking (1992), A model of nitrous oxide evolution from soil driven by rainfall events: 1. Model structure and sensitivity, *J. Geophys. Res.*, *97*(D9), 9759–9776, doi:10.1029/92JD00509.
- Li, C., S. Frolking, and R. Harriss (1994), Modeling carbon biogeochemistry in agricultural soils, *Global Biogeochem. Cycles*, *8*(3), 237–254, doi:10.1029/94GB00767.
- Linquist, B. A., S. M. Brouder, and J. E. Hill (2006), Winter straw and water management effects on soil nitrogen dynamics in California rice systems, *Agron. J.*, *98*(4), 1050–1059, doi:10.2134/agronj2005.0350.
- Linquist, B. A., J. E. Hill, R. G. Mutters, C. A. Greer, C. Hartley, M. D. Ruark, and C. van Kessel (2009), Assessing the necessity of surface-applied preplant nitrogen fertilizer in rice systems, *Agron. J.*, *101*(4), 906–915, doi:10.2134/agronj2008.0230x.
- Linquist, B. A., M. A. Adviento-Borbe, C. M. Pittelkow, C. van Kessel, and K. J. van Groenigen (2012a), Fertilizer management practices and greenhouse gas emissions from rice systems: A quantitative review and analysis, *Field Crop Res.*, *135*, 10–21, doi:10.1016/j.fcr.2012.06.007.
- Linquist, B., K. J. van Groenigen, M. A. Adviento-Borbe, C. Pittelkow, and C. van Kessel (2012b), An agronomic assessment of greenhouse gas emissions from major cereal crops, *Global Change Biol.*, *18*(1), 194–209, doi:10.1111/j.1365-2486.2011.02502.x.
- Liu, L., and T. L. Greaver (2009), A review of nitrogen enrichment effects on three biogenic GHGs: The CO<sub>2</sub> sink may be largely offset by stimulated N<sub>2</sub>O and CH<sub>4</sub> emissions, *Ecol. Lett.*, *12*(10), 1103–1117, doi:10.1111/j.1461-0248.2009.01351.x.
- Lu, W. F., W. Chen, B. W. Duan, W. M. Guo, Y. Lu, R. S. Lantin, R. Wassmann, and H. U. Neue (2000a), Methane emissions and mitigation options in irrigated rice fields in southeast China, *Nutr. Cycling Agroecosyst.*, *58*(1–3), 65–73, doi:10.1023/A:1009830232650.
- Lu, Y., R. Wassmann, H.-U. Neue, and C. Huang (2000b), Dynamics of dissolved organic carbon and methane emissions in a flooded rice soil, *Soil Sci. Soc. Am. J.*, *64*(6), 2011–2017, doi:10.2136/sssaj2000.6462011x.
- Myhre, G., et al. (2013), 2013: Anthropogenic and natural radiative forcing, in *Climate Change 2013: The Physical Science Basis, Contribution of Working Group I to the Fifth Assessment Report of the Intergovernmental Panel on Climate Change*, edited by T. F. Stocker et al., pp. 659–740, Cambridge Univ. Press, Cambridge, U. K., and New York.

- Pathak, H., C. Li, and R. Wassmann (2005), Greenhouse gas emissions from Indian rice fields: Calibration and upscaling using the DNDC model, *Biogeosciences*, 2, 113–123, doi:10.5194/bg-2-113-2005.
- Peng, S., and K. G. Cassman (1998), Upper thresholds of nitrogen uptake rates and associated nitrogen fertilizer efficiencies in irrigated rice, *Agron. J.*, 90(2), 178–185, doi:10.2134/agronj1998.0002196200900020010x.
- Peng, S., et al. (2010), Improving nitrogen fertilization in rice by site-specific N management, *Agron. Sustainable Dev.*, 30(3), 649–656, doi:10.1051/agro/2010002.
- Peoples, M. B., and E. T. Craswell (1992), Biological nitrogen fixation: Investments, expectations and actual contributions to agriculture, *Plant Soil*, 141(1–2), 13–39, doi:10.1007/BF00011308.
- Pittelkow, C. M., M. A. Adviento-Borbe, J. E. Hill, J. Six, C. van Kessel, and B. A. Linquist (2013), Yield-scaled global warming potential of annual nitrous oxide and methane emissions from continuously flooded rice in response to nitrogen input, *Agric. Ecosyst. Environ.*, 177, 10–20, doi:10.1016/j.agee.2013.05.011.
- Pittelkow, C. M., M. A. Adviento-Borbe, C. van Kessel, J. E. Hill, and B. A. Linquist (2014a), Optimizing rice yields while minimizing yield-scaled global warming potential, *Global Change Biol.*, 20(5), 1382–1393, doi:10.1111/gcb.12413.
- Pittelkow, C. M., Y. Assa, M. Burger, R. G. Mutters, C. A. Greer, L. A. Espino, J. E. Hill, W. R. Horwath, C. van Kessel, and B. A. Linquist (2014b), Nitrogen management and methane emissions in direct-seeded rice systems, *Agron. J.*, 106(3), 968–980, doi:10.2134/agronj13.0491.
- Ponnamperuma, F. N. (1981) Some aspects of the physical chemistry of paddy soils, in *Proceedings of Symposium on Paddy Soil*, edited by A. Sinica, pp. 59–94, Science Press-Springer, Beijing, China, and Berlin, Germany, doi:10.1007/978-3-642-68141-7\_5.
- Schimel, J. (2000), Global change: Rice, microbes, and methane, *Nature*, 403, 375–377, doi:10.1038/35000325.
- Shiratori, Y., H. Watanabe, Y. Furukawa, H. Tsuruta, and K. Inubushi (2007), Effectiveness of a subsurface drainage system in poorly drained paddy fields on reduction of methane emissions, *Soil Sci. Plant Nutr.*, 50(4), 387–400, doi:10.1111/j.1747-0765.2007.00171.x.
- Simmonds, M. B., R. E. Plant, J. M. Peña-Barragán, C. van Kessel, J. Hill, and B. A. Linquist (2013), Underlying causes of yield spatial variability and potential for precision management in rice systems, *Precision Agric.*, 14(5), 512–540, doi:10.1007/s11119-013-9313-x.
- Simmonds, M. B., M. Anders, M. A. Adviento-Borbe, C. van Kessel, A. McClung, and B. A. Linquist (2015), Seasonal methane and nitrous oxide emissions of several rice cultivars in direct-seeded systems, *J. Environ. Qual.*, 44(1), 103–114, doi:10.2134/jeq2014.07.0286.
- Smith, P., et al. (2007), 2007: Agriculture, in *Climate Change 2007: Mitigation. Contribution of Working Group III to the Fourth Assessment Report of the Intergovernmental Panel on Climate Change*, edited by B. Metz et al., pp. 497–540, Cambridge Univ. Press, Cambridge, U. K., and New York.
- Stange, F., K. Butterbach-Bahl, H. Papen, S. Zechmeister-Boltenstern, C. S. Li, and J. Aber (2000), A process-oriented model of N<sub>2</sub>O and NO emissions from forest soils: 2. Sensitivity analysis and validation, *J. Geophys. Res.-Atmos.*, 105(D4), 4385–4398, doi:10.1029/1999JD900948.
- Tyler, S. C., R. S. Bilek, R. L. Sass, and F. M. Fisher (1997), Methane oxidation and pathways of production in a Texas paddy field deduced from measurements of flux,  $\delta^{13}\text{C}$ , and  $\delta\text{D}$  of CH<sub>4</sub>, *Global Biogeochem. Cycles*, 11(3), 323–348, doi:10.1029/97GB01624.
- United States Environmental Protection Agency (2014), *Inventory of U.S. Greenhouse Gas Emissions and Sinks: 1990–2012*, U.S. Environmental Protection Agency, Washington, D. C.
- van Bodegom, P. M., and J. C. M. Scholten (2001), Microbial processes of CH<sub>4</sub> production in a rice paddy soil: Model and experimental validation, *Geochim. Acta*, 65(13), 2055–2066, doi:10.1016/S0016-7037(01)00563-4.
- Wang, J., X. Zhang, Z. Xiong, M. A. K. Khalil, X. Zhao, Y. Xie, and G. Xing (2012), Methane emissions from a rice agroecosystem in South China: Effects of water regime, straw incorporation, and nitrogen fertilizer, *Nutr. Cycling Agroecosyst.*, 93(1), 103–112, doi:10.1007/s10705-012-9503-3.
- Wang, Z. P., C. W. Lindau, R. D. Delaune, and W. H. Patrick Jr. (1993), Methane emission and entrapment in flooded rice soils as affected by soil properties, *Biol. Fertil. Soils*, 16(3), 163–168, doi:10.1007/BF00361401.
- Watanabe, A., and M. Kimura (1998), Effect of rice straw application on CH<sub>4</sub> emission from paddy fields: IV. Influence of rice straw incorporated during the previous cropping period, *Soil Sci. Plant Nutr.*, 44(4), 507–512, doi:10.1080/00380768.1998.10414474.
- Xie, B., et al. (2010), Effects of nitrogen fertilizer on CH<sub>4</sub> emission from rice fields: Multi-site field observations, *Plant Soil*, 326(1–2), 393–401, doi:10.1007/s11104-009-0020-3.
- Xu, H., and Y. Hosen (2010), Effects of soil water content and rice straw incorporation in the fallow season on CH<sub>4</sub> emissions during fallow and the following rice-cropping seasons, *Plant Soil*, 335(1–2), 373–383, doi:10.1007/s11104-010-0426-y.
- Xu, H., Z. C. Cai, X. P. Li, and H. Tsuruta (2000), Effect of antecedent soil water regime and rice straw application time on CH<sub>4</sub> emission from rice cultivation, *Aust. J. Soil Res.*, 38(1), 1–12, doi:10.1071/SR99026.
- Xu, H., Z. C. Cai, and H. Tsuruta (2003), Soil moisture between rice growing seasons affects methane emission, production, and oxidation, *Soil Sci. Soc. Am. J.*, 67(4), 1147–1157, doi:10.2136/sssaj2003.1147.
- Xu, X., Y. Kuzyakov, W. Wanek, and A. Richter (2008), Root-derived respiration and non-structural carbon of rice seedlings, *Eur. J. Soil Sci.*, 44(1), 22–29, doi:10.1016/j.ejsobi.2007.09.008.
- Yan, X., K. Yagi, H. Akiyama, and H. Akimoto (2005), Statistical analysis of the major variables controlling methane emission from rice fields, *Global Change Biol.*, 11(7), 1131–1141, doi:10.1111/j.1365-2486.2005.00976.
- Yao, H., R. Conrad, R. Wassmann, and H. U. Neue (1999), Effect of soil characteristics on sequential reduction and methane production in sixteen rice paddy soils from China, the Philippines, and Italy, *Biogeochemistry*, 47(3), 269–295, doi:10.1007/BF00992910.
- Yao, Z., X. Zheng, H. Dong, R. Wang, B. Mei, and J. Zhu (2012), A 3-year record of N<sub>2</sub>O and CH<sub>4</sub> emissions from a sandy loam paddy during rice seasons as affected by different nitrogen application rates, *Agric. Ecosyst. Environ.*, 152, 1–9, doi:10.1016/j.agee.2012.02.004.
- Yu, K. W., Z. P. Wang, and G. X. Chen (1997), Nitrous oxide and methane transport through rice plants, *Biol. Fertil. Soils*, 24(3), 341–343, doi:10.1007/s003740050254.
- Zehnder, A. J. B., and W. Stumm (1988), Geochemistry and biogeochemistry of anaerobic habitats, in *Biology of Anaerobic Microorganisms*, edited by A. J. B. Zehnder, pp. 1–38, Wiley, New York.
- Zhang, Y., C. Li, C. C. Trettin, H. Li, and G. Sun (2002a), An integrated model of soil, hydrology, and vegetation for carbon dynamics in wetland ecosystems, *Global Biogeochem. Cycles*, 16(4), 1061, doi:10.1029/2001GB001838.
- Zhang, Y., C. Li, X. Zhou, and B. Moore III (2002b), A simulation model linking crop growth and soil biogeochemistry for sustainable agriculture, *Ecol. Modell.*, 151(1), 75–108, doi:10.1016/S0304-3800(01)00527-0.